Received: 21 December 2020 | Revised: 19 March 2021 | Accepted: 2 April 2021

DOI: 10.1002/ar.24747

SPECIAL ISSUE ARTICLE

The Anatomical Record

WILEY

Picking up the threads: Comparative osteology and associated cartilaginous elements for members of the genus *Trilepida* Hedges, 2011 (Serpentes, Leptotyphlopidae) with new insights on the Epictinae systematics

Angele Martins[1,2] | **Claudia Koch**[3] | **Mitali Joshi**[3] | **Roberta Pinto**[4] | **Paulo Passos**[2]

[1]Departamento de Ciências Fisiológicas, Universidade de Brasília, Brasília, Brazil

[2]Departamento de Vertebrados, Museu Nacional, Universidade Federal do Rio de Janeiro, Rio de Janeiro, Brazil

[3]Zoologisches Forschungsmuseum Alexander Koenig, Bonn, Germany

[4]Laboratório de Diversidade de Anfíbios e Répteis, Museu de Arqueologia da Universidade Católica de Pernambuco, Universidade Católica de Pernambuco, Recife, Brazil

Correspondence
Angele Martins, Laboratório de Anatomia Comparada de Vertebrados, Departamento de Ciências Fisiológicas, Instituto de Ciências Biológicas, Campus Darcy Ribeiro, Universidade de Brasília, Asa Norte, Brasília, Distrito Federal 70910-900, Brazil.
Email: amartins@unb.br

Funding information
Conselho Nacional de Desenvolvimento Científico e Tecnológico (CNPq), Grant/Award Number: #309560/2018-7; Fundação Carlos Chagas Filho de Amparo à Pesquisa do Estado do Rio de Janeiro (FAPERJ), Grant/Award Numbers: #E-26/202.403/2017, #E-26/202.737/2018, #E-26/211.154/2019; Smithsonian Institution (SI), Grant/Award Number: Short Term Fellowship 2015; Coordenação de Aperfeiçoamento de Pessoal de Nível Superior (CAPES), Grant/Award Number: #99999.010032/2014-02

Abstract

The threadsnakes of the family Leptotyphlopidae have been historically neglected in terms of their natural history, ecology, systematics, and morphology. Given the relevance of morphological data for resolving systematic, evolutionary, and functional issues, we aimed to provide a detailed comparative description of osteology and associated cartilaginous elements for members of the genus *Trilepida*. Data were obtained through high-resolution computed tomography images, cleared and stained specimens, and radiography images of a total of 47 specimens and 12 species. Both cranial and axial osteology characters exhibited a relevant degree of intraspecific variation regarding qualitative and quantitative data associated with skull and vertebrae foramina and the shape of bony sutures and processes. The high representativeness of examined species and specimens allows us to provide a comprehensive discussion on the inter- and intraspecific osteological variation, as well as a compelling osteological diagnosis for the entire genus. *Trilepida* spp. differ from all Epictinae by the presence of the following combination of characters: paired nasals, fused supraoccipitals (distinct from parietal, prootics, and otooccipitals), a single (fused) parietal without a dorsal fontanelle, and the basioccipital participating in the foramen magnum (except in *Trilepida nicefori*). Our results reinforce the need for integration of detailed anatomical traits to usually conserved external morphological data to provide accurate diagnostic features for Epictinae. In addition, new phylogenetic hypotheses or even taxonomic re-allocations may broadly benefit from these detailed comparative studies.

KEYWORDS
cartilaginous elements, morphology, lower jaw, postcranial skeleton, skull, threadsnakes

1 | INTRODUCTION

The small-sized snakes known as threadsnakes (Leptotyphlopidae) comprise about 145 species with fossorial habits that occur mostly in the Neotropics (Adalsteinsson, Branch, Trape, Vitt, & Hedges, 2009; Uetz, Freed, & Hosek, 2020). As well as other burrowing taxa traditionally known as "scolecophidians" (i.e., Anomalepididae and Typhlopoidea), this lineage is known for its extreme anatomical and functional novelties mostly related to their skull and lower jaw, cephalic glands, and head muscles (Cundall & Irish, 2008; List, 1966; Martins et al., 2018; Martins, Passos, & Pinto, 2019; Rieppel, Kley, & Maisano, 2009). However, given their secretive habits and remarkably reduced size, threadsnakes have long been neglected in terms of their natural history, ecology, systematics, and morphology (Adalsteinsson et al., 2009; Greene, 1997; Wallach, 2016). Furthermore, the usually conserved external morphology exhibited by leptotyphlopids has historically hampered the recognition of external diagnostic characters for many taxa, leading to a scenario of taxonomic uncertainty for inferring species boundaries (Martins, Koch, et al., 2019; Wallach, 2016). In such a view, anatomical characters have emerged as potentially valuable data for leptotyphlopid systematics, either by providing robust morphological diagnosis (= synapomorphies) at family rank (Lee, Hugall, Lawson, & Scanlon, 2007; Lee & Scanlon, 2002; Vidal & Hedges, 2002; Wallach, 1998a), or by less inclusive levels of phylogeny like tribes and genera (= putative synapomorphies; Martins, Koch, et al., 2019), and even for allowing the description of species (= putative autapomorphies; Koch, Martins, & Schweiger, 2019).

Despite several anatomical contributions that have accumulated in the past decades (e.g. Baird, 1970; Broadley & Broadley, 1999; Broadley & Wallach, 2007; Brock, 1932; Brongersma, 1958; Duerden & Essex, 1923; Essex, 1927; Fabrezi, Marcus, & Scrocchi, 1985; FitzSimons, 1962; Gauthier, Kearney, Maisano, Rieppel, & Behlke, 2012; Kley, 2006; Kley & Brainerd, 1999; Lapage, 1928; List, 1955, 1966; Miller, 1968; Parker & Grandison, 1977; Rieppel, 1979; Rieppel et al., 2009; Van Devender & Mead, 1978; Van Devender & Worthington, 1977), descriptive and detailed morphological studies are still scarce even after more than 150 years since the first species recognition (Duméril, 1853; Jan & Sordelli, 1861; Peters, 1858). The historical time-consuming physical dissection and clearing and staining has much likely hampered the exploration of several anatomical data of threadsnakes at a large scale, mostly for rare or poorly collected taxa (Pinto, Martins, Curcio, & Ramos, 2015). However, the emergence of high-resolution computed tomography facilitated the acquisition of detailed anatomical data (mainly osteological) even for rare or insufficiently represented species in museum collections, allowing the assessment of anatomical data without the use of invasive techniques (Koch et al., 2019; Martins, Koch, et al., 2019; Pinto et al., 2015; Salazar-Valenzuela, Martins, Amador-Oyola, & Torres-Carvajal, 2015). Even with this novel and promising image acquisition method, morphological contributions on leptotyphlopids are still far from being satisfactorily explored in terms of their systematic utility, evolution, and functional morphology.

In view of the low representativeness of studies that provide detailed inter- and intraspecific osteological data for leptotyphlopids, we aim to provide detailed comparisons of the osteology and associated cartilaginous elements for nine species of the genus *Trilepida*. This genus currently comprises 15 recognized species that occur throughout both cis- and trans-Andean South America (Adalsteinsson et al., 2009; Pinto, Passos, Portilla, Arredondo, & Fernandes, 2010; Salazar-Valenzuela et al., 2015), and detailed osteological data are restricted to *Trilepida pastusa* (Salazar-Valenzuela et al., 2015) and *Trilepida salgueiroi* (Pinto et al., 2015). In addition, our representative sample allows us to provide osteological diagnosis for the entire genus based on the gathered data, including compelling evidence for transference of species into another Epictinae genus (see Koch, Martins, Pinto, & Passos, This volume).

2 | MATERIALS AND METHODS

We have examined a sample containing 47 specimens housed in the following institutions: Museu Nacional, Universidade Federal do Rio de Janeiro, Rio de Janeiro, Brazil (MNRJ); Universidade Federal do Mato Grosso, Mato Grosso, Brazil (UFMT); Museu de Zoologia, Universidade de São Paulo, São Paulo, Brazil (MZUSP); Museu Paraense Emílio Goeldi, Belém, Brazil (MPEG); Instituto Butantan, São Paulo, Brazil (IBSP); Laboratório de Zoologia de Vertebrados, Universidade Federal de Ouro Preto, Ouro Preto, Brazil (LZVUFOP); Coleção Herpetológica da Universidade de Brasília, Brasilia, Brazil (CHUNB); Museo de Zoología de la Pontificia Universidad Católica del Ecuador, Quito, Ecuador (QCAZ); United States National Museum, Smithsonian Institution, Washington DC (USNM); British Museum of Natural History, London, UK (BMNH); Zoological Collection of the Museum für Naturkunde, Berlin, Germany (ZMB); Naturhistorisches Museum Wien, Vienna, Austria (NHMW); Muséum national d'Histoire naturelle, Paris, France (MNHN); and Institut Royal des Sciences

Naturelles de Belgique, Brussels, Belgium (RBINS). We provide information on the sample sizes, specimens, and localities in the Material Examined section in the Appendix.

To assess data on both osteology and cartilaginous elements, 14 specimens pertaining to eight species were cleared and stained (see Material Examined in the Appendix) according to the protocols of Taylor and Van Dyke (1985) and Song and Parenti (1995). Additional osteological data were obtained through images of the skull of 18 specimens (corresponding to 12 species) with the aid of high-resolution μCT scanning procedures using a SkyScan 1176 High Resolution in vivo μCT available at USP, São Paulo, and either a Bruker SkyScan 1173 or SkyScan 1272, both available at the ZFMK, Bonn. The scans were conducted at an X-ray beam with 35 to 45 kV source voltage and 114 to 200 μA current without the use of a filter. Rotation steps of 0.25 to 0.4 degrees were used with a frame averaging of 4 to 6, recorded over a 180° rotation, resulting in 482 to 960 projections of 280 to 675 ms exposure time each and a total scan duration of 0 h:25 m:39 s–1 h:3 m:38 s. The magnification setup generated data with an isotropic voxel size of 6.4 to 21.3 μm. The μCT scan of the holotype of *Trilepida brasiliensis* (RBINS 2049.12594) was conducted with an UniTom (XRE) at the RBINS, Brussles, using an X-ray beam with 75 kV source voltage, no filter, frame averaging of 1, a 360° rotation, resulting in 1,800 projections of 500 ms exposure time, a total scan duration of 16 min, and an isotropic voxel size of 6.17 μm. Radiography images were taken from a total of 24 specimens pertaining to 10 species to gather data on vertebrae number and general vertebrae morphological features, and also hyoid topography and general morphology. For obtaining information on precloacal and caudal vertebrae and the position of the pelvic girdle, whole specimens were X-rayed in 2D outside of ethanol with a Faxitron X-ray LX60 at ZFMK; a Kevex PXS10-16W 130kVp 6 *Micron Spot MicroFocus X-Ray Source* at the USNM; and images were generated through the software KEVEX X-RAY *Source Control Interface* version 5.5.9.

We used Amira Visualization software (Thermo Fisher Scientific) for segmentation and to generate colored images of the lectotype of *Trilepida macrolepis* (ZMB 1434). Additional images were visualized in CTVox for Windows 64-bit version 2.6 (Bruker, μCT), and plates were made using Inkscape 1.0. When possible, type specimens (mainly holotypes and lectotypes) were considered for descriptions, and are indicated in the Material Examined section in the Appendix. We were able to assess data on 12 species of the 15 currently recognized *Trilepida* spp. (see Uetz et al., 2020; including specimens previously described in Pinto et al., 2015 and Salazar-Valenzuela et al., 2015), although only 11 species were considered for description, excluding *Trilepida guayaquilensis* . While examining μCT images of the *T. guayaquilensis* holotype (ZMB 4508), we noticed that osteological data, allied to external morphology evidence pointed out by Pinto et al. (2010), suggested that the taxon most likely pertains to another genus, and thus will not be described herein but will be briefly mentioned in the Discussion section (but see Koch et al., 2021). Considering the genus *Trilepida*, we have not described osteological data for *Trilepida anthracina*, *Trilepida brevissima*, and *Trilepida dugandi*. The species *T. pastusa* and *T. salgueiroi* have already been described in the literature (Pinto et al., 2015; Salazar-Valenzuela et al., 2015) and thus will not be included in the descriptions. These taxa were examined for the systematic discussion section and for comparative osteological diagnosis for the genus.

Anatomical terminology follows Hardaway and Williams (1976), and Persky, Smith, and Williams (1976) for costal cartilages; Langebartel (1968) for hyoid and tracheal cartilages; Bellairs and Kamal (1981) and Di Pietro et al. (2014) for nasal cartilages; Rieppel et al. (2009) for skull; Kley (2006) for suspensorium; Holman (2000) for vertebrae; and List (1966) and Palci, Hutchinon, Caldwell, Smith, and Lee (2019) for pelvic and hindlimb rudiments.

We identified the specimens based on the original descriptions and recent taxonomic studies addressing Epictinae taxonomy, such as Passos, Caramaschi, and Pinto (2006), Pinto et al. (2010), Pinto and Curcio (2011), and Pinto and Fernandes (2012, 2017). In many instances, we examined the type material, topotypes, and relevant comparative material in order to refine species' identifications. The supraspecific taxonomy adopted herein follows Wallach, Williams, and Boundy (2014) and Uetz et al. (2020), except for *T. guayaquilensis*.

Intra- and interspecific variation is provided within their respective descriptive sections, always accompanied by the percentage of specimens exhibiting this condition. As not all characters were distinguishable/observable in all examined specimens, the "*n*" and/or the percentage relates to the number of specimens of which the related character was analyzed, and thus will not always represent the total sample examined.

3 | RESULTS

3.1 | Skull

The skulls of members of the genus *Trilepida* are deeply ossified, longer than wide, and composed of the paired nasals, prefrontals, maxillae, septomaxillae, vomers,

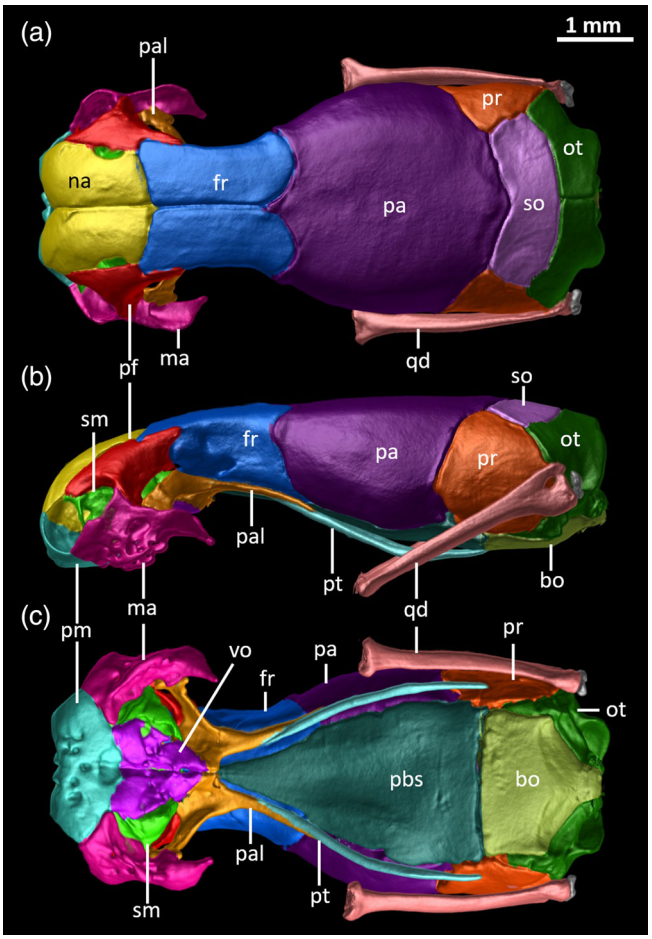

FIGURE 1 Dorsal (a), lateral (b), and ventral (c) views on the three-dimensional reconstruction of the skull of the lectotype of *Trilepida macrolepis* (ZMB 1434) based on μCT data. Different skull elements are digitally colored to improve elements visualization, and the mandible was digitally removed for better visualization. bo, basioccipital; fr, frontal; ma, maxilla; na, nasal; ot, otooccipital; pa, parietal; pal, palatine; pbs, parabasisphenoid; pf, prefrontal; pm, premaxilla; pr, prootic; pt, pterygoid; qd, quadrate; sm, septomaxilla; so, supraoccipital; vo, vomer

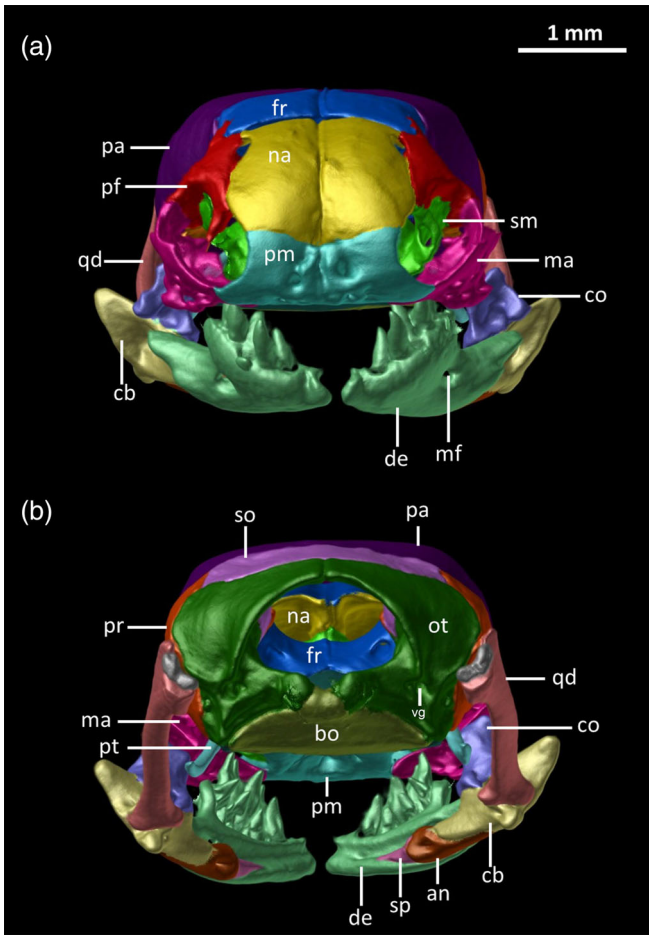

FIGURE 2 Anterior (a) and posterior (b) views on the three-dimensional reconstruction of the skull and lower jaw (suspensorium + mandible) of the lectotype of *Trilepida macrolepis* (ZMB 1434) based on μCT data. Different skull elements are digitally colored to improve elements visualization. an, angular; bo, basioccipital; cb, compound bone; co, coronoid; de, dentary; fr, frontal; ma, maxilla; na, nasal; ot, otooccipital; pa, parietal; pf, prefrontal; pm, premaxilla; pr, prootic; pt, pterygoid; qd, quadrate; so, supraoccipital; sp, splenial; vg, vagus nerve foramen

frontals, palatines, otooccipitals, prootics, and pterygoids; the following bones are single or fused into a single element: premaxilla, parietal, supraoccipital (fused and distinct from parietal), basioccipital, and parabasisphenoid (Figures 1–7).

3.1.1 | Snout complex

The snout complex is composed of the premaxilla, nasals, prefrontals, septomaxillae, vomers, and maxillae, being approximately as wide as the widest region of the braincase (parietal) (Figures 1–7). All elements are partially overlapped (i.e., telescoped; Figure 3) at some level, rendering the snout complex as a robust and akinetic structure. The naris is anterolaterally oriented and limited by the premaxilla anteriorly and ventrally, the septomaxilla posteriorly, and the nasal dorsally.

The nasal cartilage (Figure 8) widely overlaps the dorsal elements of the snout complex, totally covering the nasals and prefrontals ventrally, as well as a small portion of the frontals and maxillae anteriorly. The nasal cartilage also descends anteriorly and anterolaterally to cover the entire premaxilla, surrounding the naris and slightly contacting the lateral arm of the ectochoanal cartilage posteriorly (Figure 8b,c; in *Trilepida koppesi*, 100%, $n = 3$, this contact is not present). The wide dorsoposterior portion of the nasal cartilage most likely represents a well-developed *planum orbitale* that almost reaches the posterior limit of the prefrontal (Figure 8a).

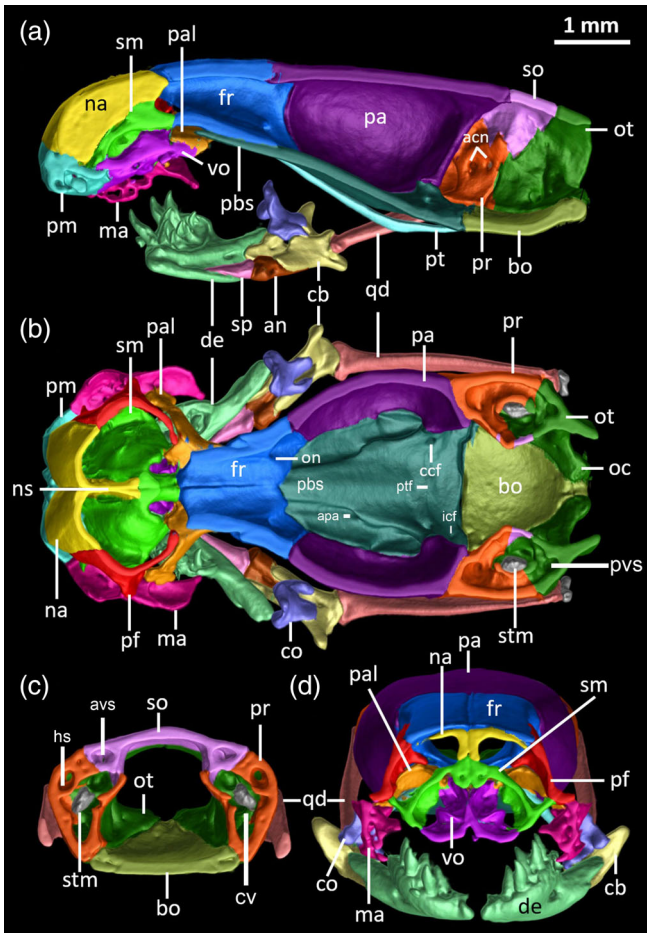

FIGURE 3 Three-dimensional cutaway views along the sagittal (a), vertical (b), and transverse (c, d) axes of the skull of the lectotype of *Trilepida macrolepis* (ZMB 1434) based on μCT data. Different skull elements are digitally colored to improve elements visualization. acn, acoustic nerve foramina; an, angular; apa, anterior palatine artery opening; avs, anterior verticula semicircular canal; bo, basioccipital; cb, compound bone; ccf, cerebral carotid foramen; co, coronoid; cv, cavum vestibuli; de, dentary; fr, frontal; hs, horizontal semicircular canal; icf, internal carotid foramen; ma, maxilla; na, nasal; ns, nasal septum; oc: occipital condyle; on, optic nerve foramen; ot, otooccipital; pa, parietal; pal, palatine; pbs, parabasisphenoid; pf, prefrontal; pm, premaxilla; pr, prootics; pt, pterygoid; ptf, pituitary fossa; pvs, posterior vertical semicircular canal; qd, quadrate; sm, septomaxilla; so, supraoccipital; sp, splenial; stm, statolithic mass; vo, vomer

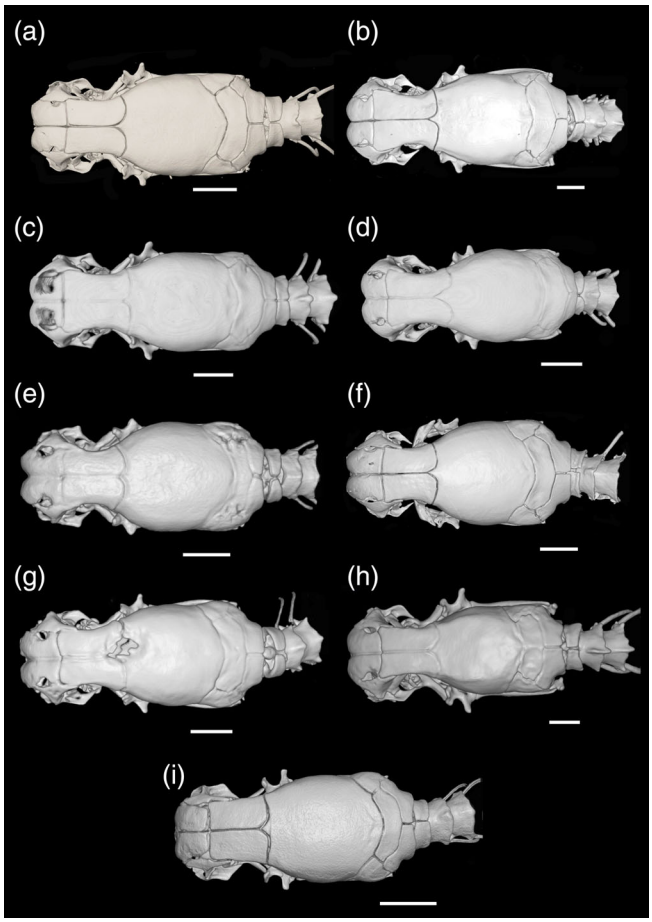

FIGURE 4 Three-dimensional reconstruction of the skull, cervical vertebrae and first trunk vertebrae of *Trilepida* spp. in dorsal view. (a) *T. affinis* (BMNH 1946.1.11.16); (b) *T. brasiliensis* (RBINS 2049.12594); (c) *T. dimidiata* (MZUSP 10120); (d) *T. fuliginosa* (MNRJ 19223); (e) *T. jani* (LZV 778S); (f) *T. joshuai* (NHMW 38424.2); (g) *T. koppesi* (MNRJ 24716); (h) *T. macrolepis* (ZMB 5294); and (i) *T. nicefori* (MNHN 1900.151). Scale bars = 1 mm

The fenestra found in this cartilage seems to represent a posteriorly displaced *fenestra olfactoria advehens* that is topographically close to the apicalis nerve foramen (Figure 8a). The expanded dorsoanterior portion might represent the lateral expansion of the parietotectal cartilage. The ventroanterior cartilaginous expansion that delimits the premaxilla represents a well-developed inferior alary process that is associated with a robust and wide premaxilla (Figure 8c). The inferior alary process contacts neither the vomeronasal conchal cartilage nor the nasal septum. A cartilage that articulates with the palatine is absent. The hypochoanal and ectochoanal cartilages are well-developed, being located ventrally to the septomaxillae and vomers (Figure 8c). The ectochoanal cartilages are Y-shaped structures that connect posteriorly to the boot-shaped hypochoanal cartilage (Figure 8c), and might exhibit internal points of ossification (*Trilepida jani*, 100%, $n = 2$; *T. koppesi*, 100%, $n = 3$) or be conspicuously ossified (*Trilepida fuliginosa*, 100%, $n = 2$).

The premaxilla (Figures 1–3, 6, and 7) is edentulous and forms the anteroventral portion of the snout complex. It contacts the nasals dorsally, the vomers ventroposteriorly, and both the septomaxillae and maxillae ventrolaterally. A variable number of foramina, ranging

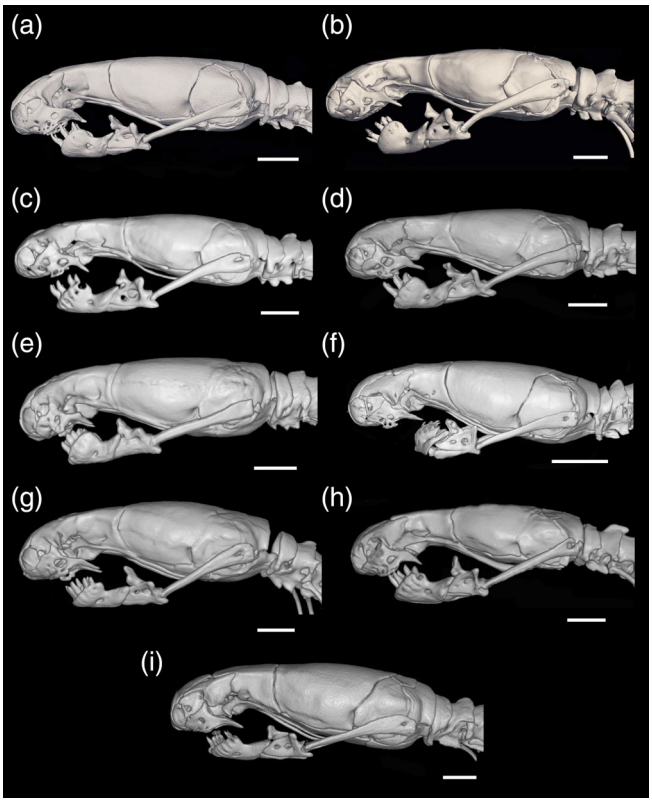

FIGURE 5 Three-dimensional reconstruction of the skull of *Trilepida* spp. in lateral view. (a) *T. affinis* (BMNH 1946.1.11.16); (b) *T. brasiliensis* (RBINS 2049.12594); (c) *T. dimidiata* (MZUSP 10120); (d) *T. fuliginosa* (MNRJ 19221); (e) *T. jani* (LZV 778S); (f) *T. joshuai* (NHMW 38424.2); (g) *T. koppesi* (MNRJ 24716); (h) *T. macrolepis* (ZMB 5294); and (i) *T. nicefori* (MNHN 1900.151). Scale bars = 1 mm

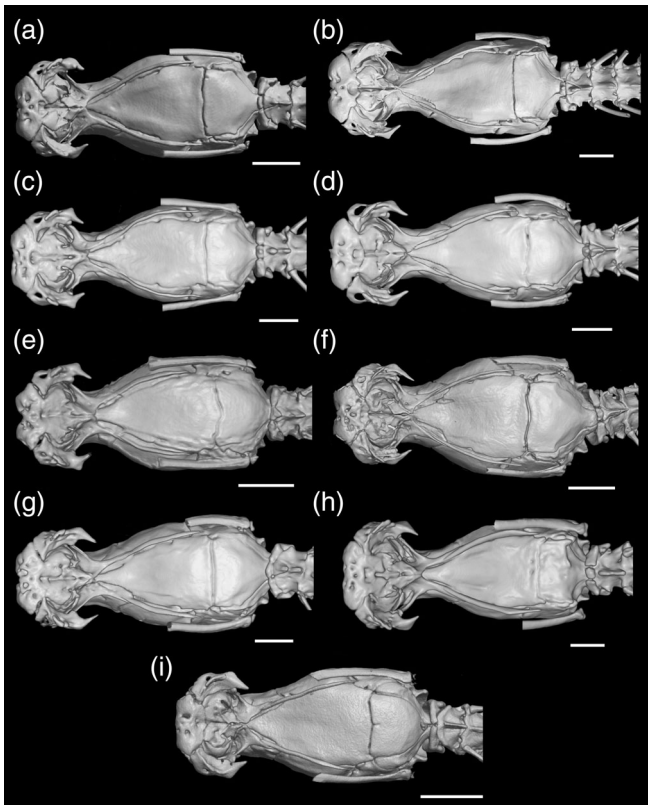

FIGURE 6 Three-dimensional reconstruction of the skull of *Trilepida* spp. in ventral view. The mandible and part of the quadrate were digitally removed for better visualization of ventral skull elements. (a) *T. affinis* (BMNH 1946.1.11.16); (b) *T. brasiliensis* (RBINS 2049.12594); (c) *T. dimidiata* (MZUSP 10120); (d) *T. fuliginosa* (MNRJ 19221); (e) *T. jani* (LZV 778S); (f) *T. joshuai* (NHMW 38424.2); (g) *T. koppesi* (MNRJ 24716); (h) *T. macrolepis* (ZMB 5294); and (i) *T. nicefori* (MNHN 1900.151). Scale bars = 1 mm

from 4 to 10 (see Table 1) and recesses in the premaxilla give path to the rami of the *ophthalmicus profundus* nerve (V1; Haas, 1964), varying both inter- and intraspecifically (Figures 1–2, 6, and 7). The anterior lamina of the premaxilla is approximately rectangular with concave lateral limits (Figures 2 and 7), and the dorsal limit that contacts the nasals is straight or oblique (Figures 2 and 7), usually hardly visible in dorsal view (Figures 2 and 7; see Table 1 for variation). An internasal process that projects dorsally and fits medially between the paired nasals is usually absent (Figures 1 and 7a–c), but in a few species/specimens, this reduced triangular projection is present (Figure 7e,f; Table 1). Short anterior transverse processes may occur in the *Trilepida* spp. (Table 1). The ventral lamina of the premaxilla expands posteriorly into a vomerine process that is usually tapered, except in one specimen of *T. jani* (33%), with its posterior limit being narrower than the anterior limits in ventral view (Figures 1 and 6). In most specimens, the midposterior region of the vomerine process exhibits double medial projections (Figures 1 and 6, except Figure 6d, f), but in one specimen of *Trilepida joshuai* (50%, Figure 6f) and one of *T. macrolepis* (33%), it might exhibit three inconspicuous projections, or a single tapered projection in *T. fuliginosa* (50%, $n = 1$; Figure 6d). The premaxilla also receives each maxilla ventrolaterally, loosely attaching to its lateral edges.

The paired nasals (Figures 1–7) are approximately rectangular, being longer than wide in dorsal view (Figures 1 and 4; see Table 1). Each nasal contacts the premaxilla anteriorly and ventrally, the frontal posteriorly and prefrontal lateroposteriorly, and the septomaxillae medially. The nasal-frontal suture is usually straight and transversal, but in one specimen of *T. brasiliensis* it is slightly and almost imperceptibly concave (25%), while in *T. macrolepis* it is most commonly slightly oblique (Figures 1a and 4h; 75%, $n = 3$). The variation in the nasal-premaxilla suture is described in "premaxilla." The dorsal surface of the nasals is essentially convex, with each element projecting midventrally

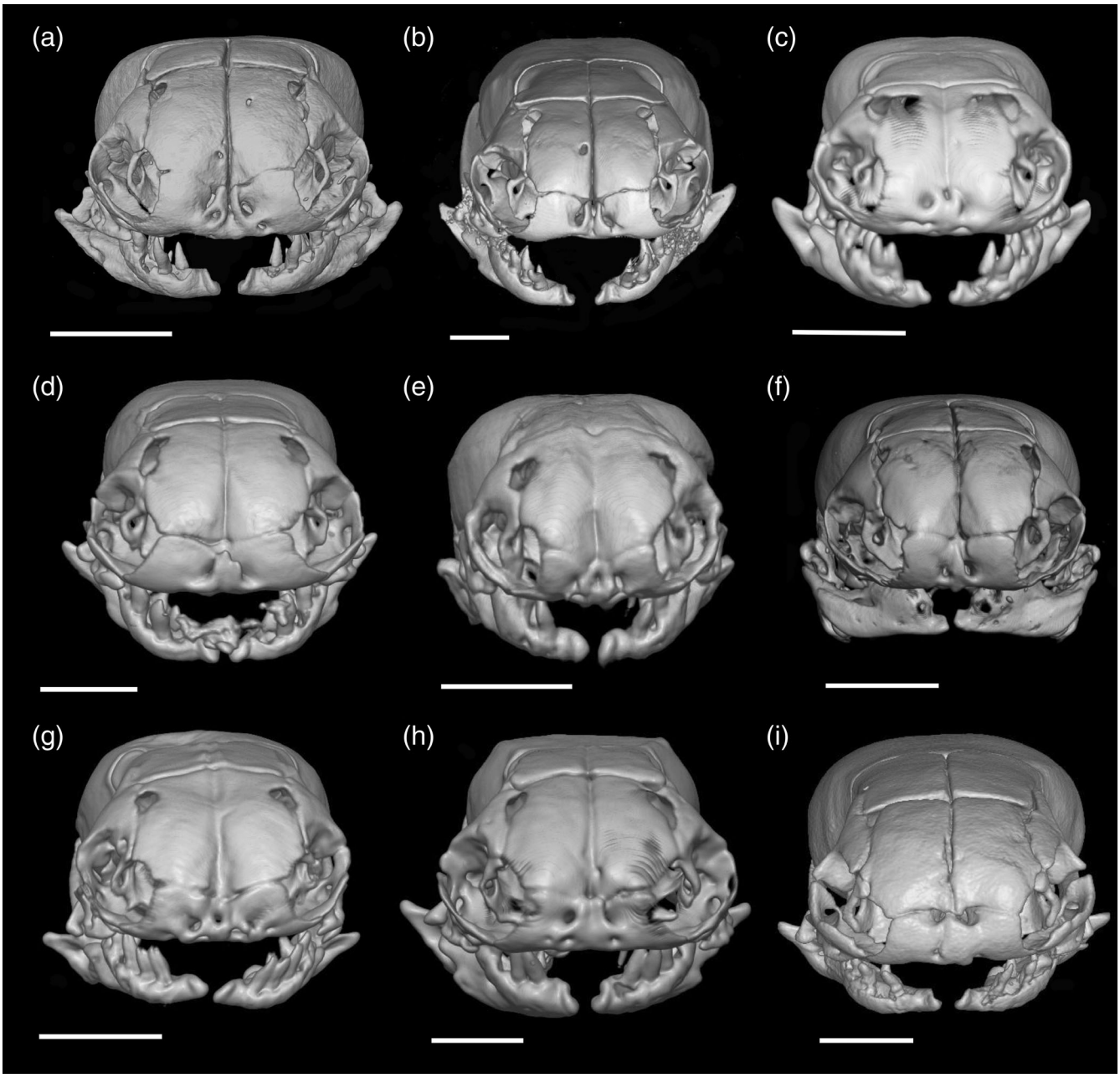

FIGURE 7 Three-dimensional reconstruction of the skull of *Trilepida* spp. in anterior view. (a) *T. affinis* (BMNH 1946.1.11.16); (b) *T. brasiliensis* (RBINS 2049.12594); (c) *T. dimidiata* (MZUSP 10120); (d) *T. fuliginosa* (MNRJ 19221); (e) *T. jani* (LZV 778S); (f) *T. joshuai* (NHMW 38424.2); (g) *T. koppesi* (MNRJ 24716); (h) *T. macrolepis* (ZMB 5294); and (i) *T. nicefori* (MNHN 1900.151). Scale bars = 1 mm

forming the paired nasal septum that is ventrally supported by the short medial (internal) lamina of the premaxilla (Figure 3). Each nasal participates, with the prefrontal, in the formation of the foramen for the *apicalis nasi* nerve (Figures 1a, 4, and 7). In *T. nicefori*, the frontals also participate in the formation of the posterior margin of this foramen (Figures 4i and 7i). A single additional foramen might be present in the left nasal (*Trilepida affinis*, 100%, $n = 1$; *T. brasiliensis*, 33%, $n = 1$; *T. joshuai*, 100%, $n = 3$) and the right nasal (*T. affinis*, 100%, $n = 1$; *T. brasiliensis*, 100%, $n = 1$; *Trilepida dimidiata*, 100%, $n = 2$; *T. nicefori*, 100%, $n = 1$; Figure 4f). In one specimen of *T. dimidiata* (33%), the left nasal is pierced by two wide additional foramina.

The prefrontals (Figures 1–7) are irregular, located laterally to the snout complex. Each element contacts the nasal, the frontal, and the ascending process of the septomaxilla medially, the maxilla ventrally and, in a few specimens, the palatine posteriorly. Each prefrontal bears three processes: an anterior process (nasal process),

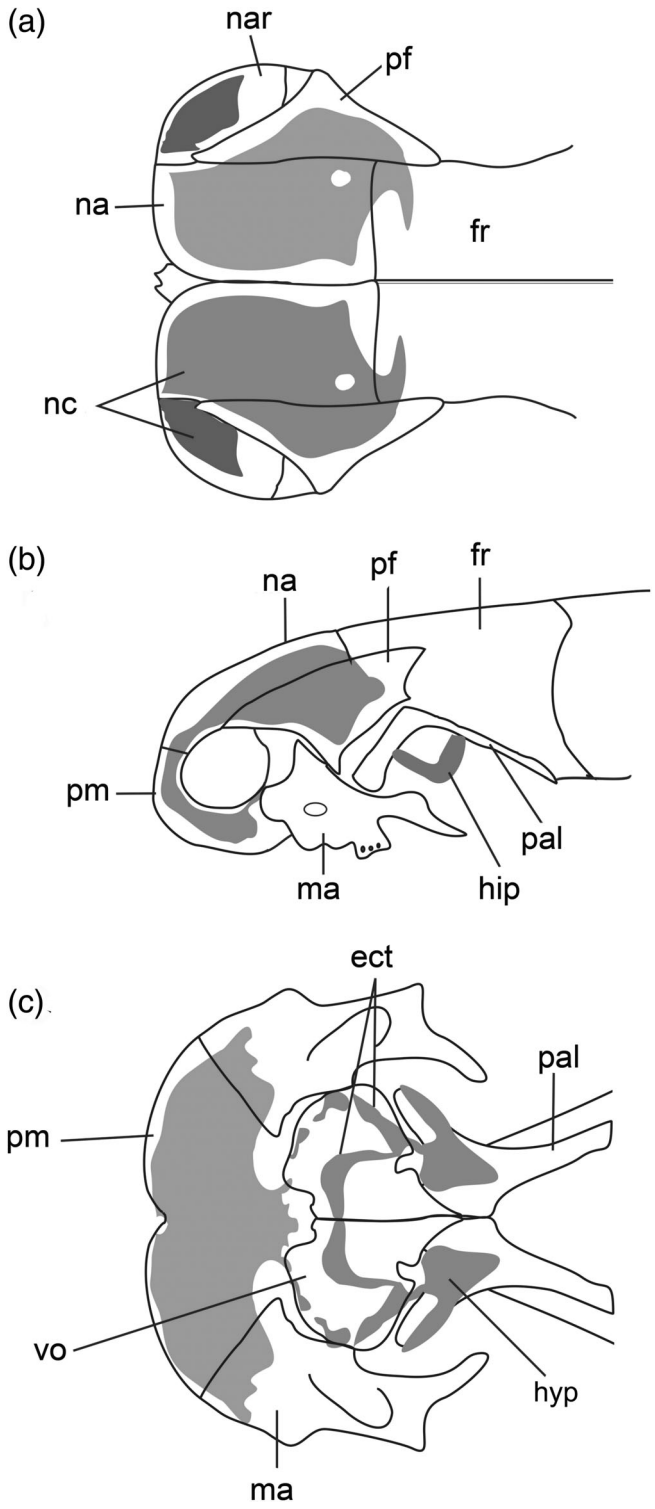

FIGURE 8 Dorsal (a), lateral (b), and ventral (c) views based on the schematic illustration of the snout complex of a cleared and stained specimen of *Trilepida brasiliensis* (UFMT 1163), with details on nasal, hypochoanal, and ectochoanal cartilages. Gray elements represent cartilaginous (blue-stained) elements. ect, ectochoanal cartilage; fr, frontal; hyp, hypochoanal cartilage; ma, maxilla; na, nasal; nar, naris; nc, nasal cartilage; pal, palatine; pf, prefrontal; pm, premaxilla; vo, vomer

a posterior process (frontal process), and a ventral process (maxillary process). Both nasal and frontal processes are short anterior and posterior projections that contact the nasals and frontals respectively (Figures 1, 4, and 5). The maxillary process descends to form concave anteroventral and posteroventral surfaces with the former, contacting the maxilla laterally, and the ascending process of the septomaxilla anteroventrally (Figures 1b and 5). This triad of contact creates a recess that accommodates the nasal gland (Martins et al., 2018; Rieppel et al., 2009). This recess is anteroventrally oriented in most species (*T. brasiliensis*, 100%, $n = 2$; *T. dimidiata*, 67%, $n = 2$; *T. fuliginosa*, 50%, $n = 1$; *T. joshuai*, 50%, $n = 1$; *T. koppesi*, 100%, $n = 4$; *T. macrolepis*, 100%, $n = 4$; *T. nicefori*, 100%, $n = 1$), although it is almost totally ventral in *T. affinis* (100%, $n = 1$), *T. fuliginosa* (50%, $n = 1$), *T. joshuai* (50%, $n = 1$), and *T. dimidiata* (33%, $n = 2$). The posterior lamina of the maxillary process delimits the optic capsule anteriorly (Figures 1b and 5), and in most cases (except in *T. affinis*, 100%, $n = 1$; *T. dimidiata*, 50%, $n = 1$; *T. joshuai*, 50%, $n = 1$; *T. nicefori*, 100%, $n = 1$), it also contacts the palatine ventrally. Finally, in one specimen of *T. macrolepis* (50%), the maxillary process exhibits a posterior process that is dorsally oriented, while in one specimen of *T. joshuai* (50%), this lamina is perforated by a single foramen, which is absent in all other *Trilepida* spp. examined herein.

The septomaxillae (Figures 1–7) are complex in shape, representing the main bony structure that encloses the vomeronasal organ. These elements are mostly visible in ventral view occurring dorsolaterally to the vomer, contacting all elements of the snout complex and the frontals. Each septomaxilla expands dorsolaterally originating an ascending process that slightly inflects medially toward the nasal septum (Figures 1a and 7). This ascending process contacts the prefrontal and nasal dorsally, except for *T. joshuai* (50%, $n = 1$), also being perforated by a wide anterior foramen. The ventral portion of the septomaxillae contacts the vomers to form the vomeronasal cupola. The vomeronasal cupola surrounds the vomeronasal organ and the mushroom body (Figures 1c, 3, and 6). In *T. joshuai* (100%, $n = 2$; Figure 6f), *T. koppesi* (100%, $n = 3$; Figure 6g), *T. macrolepis* (33%, $n = 1$; Figure 6h) and *T. nicefori* (100%, $n = 1$; Figure 6i), the septomaxillae do not contact the posterior wings of the vomers in ventral view. Medially (internally), each septomaxilla develops a wide lamina that forms the dorsal cover of the vomeronasal cupola (Figure 3). This lamina expands dorsoposteriorly, inflecting medially forming, together with the subolfactory process of the frontal, the passage for

TABLE 1 Inter- and intraspecific variation in the elements of the snout complex of *Trilepida spp*. (1) Total number of foramina in the premaxilla; (2) orientation of premaxilla-nasal contact; (3) anterior transverse process of the premaxilla; (4) internasal process of the premaxilla. The numbers in parentheses represent the numbers of specimens examined.

Species	1	2	3	4
T. affinis	8 (1)	O (1)	A (1)	A (1)
T. brasiliensis	5 (1), 7 (1), 8 (2)	T (1), O (2)	A (2), P-VD (3)	A (4)
T. dimidiata	10 (2)	T (1), O (1)	A (1), P-NVD (1)	A (2)
T. fuliginosa	5 (2), 6 (1)	O (2)	P-VD (2), P-NVD (1)	A (1), P (2)
T. jani	5 (2), 6 (1)	O (1)	A (1), P-NVD (2)	P (3)
T. joshuai	6 (1), 7 (1)	T (2)	A (1), P-NVD (1)	P (2)
T. koppesi	4 (1), 7 (2), 10 (1)	O (1)	P-VD (4)	A (1), P (3)
T. macrolepis	7 (1), 8 (1), 10 (1)	O (3)	A (3)	A (3)
T. nicefori	6 (1)	T (1)	A (1)	A (1)

Abbreviations: A, absent; NVD, not visible in dorsal view; O, oblique; P, present; T, transversal and straight; VD, visible in dorsal view.

the vomeronasal nerve (Figure 3b). The dorsal (= internal) lamina of the septomaxilla contacts the premaxilla anteriorly and the nasal septum posteriorly (Figure 3a). Although the dorsal lamina is usually in contact with the nasal septum throughout its whole extension, in *T. affinis* (100%, $n = 1$), it only occurs at short areas in its posterior and anterior limits. This internal lamina is also usually pierced by an anterior and a posterior foramen, whereby the anterior one leads to the internal cavity of the premaxilla. These foramina are indistinct or absent in *T. fuliginosa* (50%, $n = 1$), *T. jani* (100%, $n = 1$), *T. joshuai* (50%, $n = 1$), and *T. koppesi* (100%, $n = 1$). The dorsal surface of this internal lamina is usually grooved by the sulcus for the medial *ophthalmicus profundus* (VI; Figure 3b), although it is absent or indistinct in *T. joshuai* (50%, $n = 1$) and *T. koppesi* (100%, $n = 1$).

The vomers (Figures 1, 3, and 6) are small elements located midventrally to the vomeronasal cupola, participating in the midventral margin of the vomeronasal organ opening (*fenestra vomeronasalis*). Each vomer is pierced by a vomerine foramen, and contacts the premaxilla anteriorly, the septomaxilla laterally, and the palatine posteriorly, with its anterior limit being partially covered by the vomerine process of the premaxilla (Figures 1c and 6). The lateral wing of each vomer is wide, exhibiting a short posterior process that occludes the *fenestra vomeronasalis* and bends dorsally (internally). A posterior wing (= posterior process) is also present in each vomer, extending posteriorly to contact the palatine laterally (Figures 1c and 6). These wings might be in medial contact with each other along their entire extension, or exhibit an anterior–posterior distancing, with this variation occurring both inter- and intraspecifically. A short ventral process (= transverse process) is also present at the posterior wing of each vomer.

3.1.2 | Palatomaxillary apparatus

The palatomaxillary apparatus is composed of the paired maxillae, palatines, and pterygoids. An ectopterygoid is absent or indistinct (Figures 1–7).

The maxillae are irregular, laterally compressed, and edentulous bones that are longitudinally oriented with the skull (Figures 1–7). Each maxilla provides a ventrolateral cover for the snout complex, being connected to both the premaxilla midventrally and the prefrontal dorsally. Three distinct processes might be distinguishable in each maxilla (Figures 1b and 5): (a) a lateral lamina that abuts to the prefrontal through a dorsal triangular process and to the premaxilla by a wide dorsal and anterior process respectively, being perforated by a variable number of foramina (1–5; see Table 2) that are usually larger than the foramina of the dentigerous process; (b) a moderately developed dentigerous process that is laterally compressed and represents an irregularly vertical crest perforated by a variable number of foramina that might vary from 1 to 6 (see Table 2); and (c) a posterior tapered process that is dorsoventrally compressed, extending posteriorly and medially to the level of the optic foramen in lateral view (Table 2). The lateral lamina is usually well-developed, expanded dorsally, anteriorly covering completely or almost completely the ascending process of the septomaxilla in lateral view, or being relatively reduced and concave anteriorly in *T. brasiliensis* (100%, $n = 2$), *T. jani* (100%, $n = 1$), *T. joshuai* (100%, $n = 3$), *T. koppesi* (100%, $n = 3$), *T. macrolepis* (75%, $n = 3$), and *T. nicefori* (100%, $n = 1$), exposing a wide portion (vs. small portion) of the ascending process of the septomaxilla in lateral view (Figures 1b and 5). In a few specimens (see Table 2), the posterior process might contact the palatine medially.

The palatines (Figures 1, 3, 5, and 6) are triradiate, located lateroventrally to the anterior portion of the skull.

TABLE 2 Inter- and intraspecific variation in the maxillae for species of *Trilepida spp.* (1) Number of foramina in the lateral lamina; (2) number of foramina in the dentigerous process; (3) contact with the palatine; (4) posterior process reaches the level of the optic foramen in lateral view. The numbers in parentheses represent the number of specimens examined

Species	1	2	3	4
T. affinis	5 (1)	3 (1)	P (1)	Y (1)
T. brasiliensis	1 (1), 2 (2), 3 (1)	2 (1), 4 (2), 6 (1)	A (1), P (2)	Y (4)
T. dimidiata	2 (2), 3 (1)	2 (3)	A (2), P (1)	N (3)
T. fuliginosa	2 (1), 3 (1)	1 (1), 2 (1), 4 (1)	A (1), P (2)	Y (2), N (1)
T. jani	2 (1 side) (1), 4 (1 side) (1)	1 (1), 4 (2)	P (3)	Y (2), N (1)
T. joshuai	2 (1), 3 (1)	2 (2)	A (1), P (1)	N (2)
T. koppesi	1 (2)	1 (1), 2 (2), 3 (1)	A (1), P (2)	Y (4)
T. macrolepis	1 (1), 2 (1), 3 (1), 4 (1)	1 (1), 2 (2), 3 (1), 4 (1)	P (4)	N (4)
T. nicefori	1 (1)	2 (1)	A (1)	N (1)

Abbreviations: A, absent; N, no; P, present; Y, yes.

Each element is composed of three processes. The maxillary process represents a long anterolateral process that contacts the maxilla laterally (see maxilla for variation). The choanal process is a medial and dorsoventrally flattened projection that inflects ventrally to contact the posterior wing of the vomer (Figures 1c and 6). These processes are each perforated by a foramen and contact each other medially, although such a contact might not be visible in ventral view (*T. brasiliensis*, 50%, $n = 2$; *T. dimidiata*, 33%, $n = 1$; *T. joshuai*, 50%, $n = 1$; *T. koppesi*, 50%, $n = 2$; *T. macrolepis*, 100% $n = 4$; and *T. nicefori*, 100%, $n = 1$). The pterygoid process of the palatine is a long posterior process that medially abuts to a short anterior region of the pterygoid.

The pterygoids (Figures 1c, 2b, 3a, 5, and 6) are slender rod-like bones that extend throughout the ventral and lateral portion of the skull, from the level of the anterior portion of the parabasisphenoid almost reaching the anterior limit of the basioccipital. Each pterygoid slightly bends medially throughout its posterior extension, although in some specimens this bending might be more conspicuous. Each pterygoid is exclusively in contact with the pterygoid process of the palatine anteriorly, with its whole posterior extension being suspended from the skull by the *Musculus protractor pterygoidei* (Martins et al., 2018).

3.1.3 | Orbital complex and braincase

The orbital complex is limited anteriorly by the prefrontals (described above) and medially by the frontals, with the latter totally enclosing the optic foramen (Figures 1–7). A posterior orbital element is absent. The braincase is composed of the parietal, supraoccipitals, prootics, otooccipitals, parabasisphenoid complex, and basioccipital.

The frontals are wide elements that form a conspicuous anterior area of the skull, being about three times longer than wide (*T. brasiliensis*, 25%, $n = 1$; *T. dimidiata*, 33%, $n = 1$; *T. fuliginosa*, 100%, $n = 3$; *T. koppesi*, 25%, $n = 1$; *T. macrolepis*, 25%, $n = 1$) or twice as long as wide (*T. affinis*, 100%, $n = 1$; *T. brasiliensis*, 75%, $n = 3$; *T. dimidiata*, 67%, $n = 2$; *T. joshuai*, 100%, $n = 2$; *T. koppesi*, 75%, $n = 3$; *T. macrolepis*, 75%, $n = 3$; and *T. nicefori*, 100%, $n = 1$; Figures 1 and 4). Each frontal is nearly rectangular in dorsal view, with a straight (in most of the species) anterior limit (see nasals for variation), and a convex posterior limit. Each frontal contacts the posterior margin of the nasal anteriorly and the anterior margin of the parietal posteriorly, descending ventrally and contacting the parabasisphenoid, septomaxilla, and nasal septum. The frontals meet medially (internally) and dorsal to the parabasisphenoid, forming the frontal subolfactory processes (Figure 3a,b). A reduced anterolateral projection that fits to the prefrontal is present on the dorsal surface of each element in *T. brasiliensis* (33%, $n = 1$). The lateral surface of the frontal surrounds the anteriorly oriented optic nerve foramen (Figures 1b and 5). In one specimen of *T. joshuai* (50%), two foramina are located at its lateral surface (Figure 5f), being connected by a short internal canal. Based exclusively on μCT data, it is unclear whether the dorsal or ventral foramen gives passage for the optic nerve. In all specimens analyzed, the frontal pillars are absent, although a short midventral projection receives the dorsal portion of the nasal septum anteriorly.

The parietal (Figures 1–7) represents a single (fused) unit that comprises about one-half the length of the entire skull. This element is slightly longer than wide,

without any trace of a dorsal fontanelle, contacting the frontals anteriorly, the supraoccipital and prootics posteriorly, and the parabasisphenoid ventrally. Its medial anterior limit that contacts the frontals projects into a tapered and short process that separates both frontals in their posterior limit (Figures 1a and 4). The lateral walls of the parietal are conspicuously convex, and the posterior contact with the supraoccipital occurs through an irregularly convex suture (Figures 1a and 4). A shallow recess might occur (*T. dimidiata*, 67%, $n = 2$) on each side of its dorsoposterior lamina, accommodating the tendon for insertion of the *Musculus spinalis et semispinalis capitis* (Martins, Passos, et al., 2019). The parietal descends to form the lateral limit of the trigeminal nerve foramen exclusively with the prootics (*T. affinis*, 100%, $n = 1$; *T. brasiliensis*, 67%, $n = 2$; *T. dimidiata*, 100%, $n = 3$; *T. fuliginosa*, 50%, $n = 1$; *T. jani*, 67%, $n = 2$; *T. joshuai*, 50%, $n = 1$; *T. koppesi*, 50%, $n = 2$; *T. macrolepis*, 50%, $n = 2$; and *T. nicefori*, 100%, $n = 1$) or with the prootics and an inconspicuous portion of the parabasisphenoid (*T. brasiliensis*, 33%, $n = 1$; *T. fuliginosa*, 50%, $n = 1$; *T. jani*, 33%, $n = 1$; *T. joshuai*, 100%, $n = 2$; *T. koppesi*, 50%, $n = 2$; and *T. macrolepis*, 50%, $n = 2$). While in most species/specimens the trigeminal nerve foramen is wide and conspicuous, it is comparatively reduced in *T. nicefori* (100%, $n = 1$). The posterior lateral wall on each side of the parietal bends medially forming an internal pillar that is located anterior to the trigeminal nerve foramen and fits ventrally to the osseous dorsal enlargement of the parabasisphenoid (Figure 1a, b). The internal ventral wall of the parietal might also form, with the parabasisphenoid, a small foramen that most likely represents the opening for the facial nerve palatine branch foramen, which is distinct in *T. dimidiata* (100%, $n = 3$, Figure 6c), *T. joshuai* (50%, $n = 1$, Figure 6f), *T. koppesi* (25%, $n = 1$, Figure 6g), and *T. macrolepis* (25%, $n = 1$).

The parabasisphenoid complex (Figures 1c, 2a,b, and 6) is triangular, forming the majority of the basicranium, being extremely tapered anteriorly. It fits dorsally to the vomers and palatines, and ventrally to the frontal subolfactory processes, broadly contacting the anterior margin of the basioccipital posteriorly, and the frontals, parietal, and prootics laterally. Its posterior suture with the basioccipital (Figures 1c and 6) might vary both inter- and intraspecifically, being essentially concave (*T. brasiliensis*, 33%, $n = 1$), convex medially with approximately straight lateral margins (*T. affinis*, 100%, $n = 1$, Figure 6a; *T. fuliginosa*, 67%, $n = 2$; *T. jani*, 100%, $n = 3$, Figure 6e; *T. joshuai*, 100%, $n = 2$, Figure 6f; *T. koppesi*, 25%, $n = 1$), or essentially straight throughout its whole extension (*T. brasiliensis*, 67%, $n = 1$, Figure 6b; *T. dimidiata*, 100%, $n = 3$, Figure 6c; *T. fuliginosa*, 33%, $n = 1$; *T. koppesi*, 75%, $n = 2$, Figure 6g; *T. macrolepis*, 100%, $n = 4$, Figures 1c and 6h; *T. nicefori*, 100%, $n = 1$, Figure 6i). This suture might also bear short lateral projections providing attachment to the tendon of the *Musculus longissimus capitis, pars transversalis cervicis* (Martins, Passos, et al., 2019; *T. dimidiata*, 100%, $n = 1$; *T. fuliginosa*, 50%, $n = 1$; *T. jani*, 67%, $n = 2$; *T. joshuai*, 100%, $n = 2$; *T. koppesi*, 33%, $n = 1$; and *T. macrolepis*, 25%, $n = 1$, Figure 6h). A small foramen is formed on each side with the prootic, opening internally into the wide trigeminal nerve foramen. Internally, an osseous projection that fits dorsally to the parietal pillar is always present. The pituitary fossa (*sella turcica*) is shallow and located in the mid-posterior region of the parabasisphenoid. This element is perforated by a series of foramina in its dorsal (internal surface), described as follows. The pair of anterior palatine artery openings represents the anteriormost foramina of the parabasisphenoid, located slightly anterior to the pituitary fossa and the large median crest of the parabasisphenoid. These foramina are followed by anterior conspicuous sulci that most likely accommodate the *trabeculae cranii*. In one specimen of *T. brasiliensis* (25%) and one of *T. dimidiata* (33%), the anterior palatine artery openings are visible in the parabasisphenoid ventral (external) lamina. In *T. macrolepis* (75%, $n = 3$), these foramina are indistinct. The pair of primary foramina for the parabasal channel (= Vidian channel) are located anterior to the osseous projections of the parabasisphenoid. These foramina are anteriorly oriented and located posterolaterally to the internal opening of the palatine artery. The reduced foramina for the palatine branch of the facial nerve lie between the anterior and the posterior internal openings of the palatine artery, being located at the suture of the parabasisphenoid and the parietal. The carotid openings are represented by a pair of moderately developed foramina that are located midposteriorly to the posterior internal opening of the palatine artery. The dorsal surface of the parabasisphenoid is pierced by the abducens nerve foramina, which lie posterolaterally to the internal carotid. These foramina are usually obscured by the parietal-prootic contact.

The *trabeculae cranii* (visible exclusively in cleared and stained specimens) represent rod-like cartilaginous elements located posterior to the ectochoanal cartilage. This structure runs along the dorsal surface of the parabasisphenoid, merging at the eye level into a *trabecula communis*. This cartilaginous structure extends posteriorly to the level of the anterior portion of the trigeminal foramen, with the medial crest of the parabasisphenoid preventing the contact between each ramus of the *trabeculae cranii*.

The basioccipital (Figures 1–3 and 6) is a wide flat plate that broadly contacts the parabasisphenoid

anteriorly, the prootics laterally, and the otooccipitals posteriorly. In ventral view, it is wide at its anterior suture with the parabasisphenoid, gradually tapering posteriorly until ending in a blunt quadrangular process (Figure 6e,i). In *T. brasiliensis* (100%, $n = 4$, Figure 6b), *T. dimidiata* (100%, $n = 3$, Figure 6c), *T. fuliginosa* (100%, $n = 3$, Figure 6d), *T. jani* (67%, $n = 2$), *T. joshuai* (37%, $n = 1$, Figure 6f), *T. koppesi* (100%, $n = 4$, Figure 6g), and *T. macrolepis* (100%, $n = 4$, Figures 1c and 6h), the basioccipital does not gradually taper in ventral view, but its lateral limits are angular at about 45°. The variation on the parabasisphenoid-basioccipital suture was described in "parabasisphenoid complex." The blunt quadrangular posterior process of the basioccipital contributes to the formation of the foramen magnum ventrally in all species (Figures 1c, 2b, 3a,b, and 6), except in *T. nicefori* (Figure 6i). In this species, the basioccipital does not participate in the formation of the foramen magnum due to a ventral contact of the otooccipitals. In a few specimens (*T. joshuai*, 50%, $n = 1$; *T. macrolepis*, 25%, $n = 1$), the basioccipital internal surface might be pierced by a variable number of evident but extremely small foramina.

The supraoccipitals (Figures 1–4) are fused into a single smooth rod-like plate that is about twice (*T. jani*, 67%, $n = 2$), three times (*T. affinis*, 100%, $n = 1$; *T. brasiliensis*, 75%, $n = 3$; *T. dimidiata*, 100%, $n = 3$; *T. jani*, 33%, $n = 1$; *T. joshuai*, 100%, $n = 3$; *T. koppesi*, 100%, $n = 4$; *T. macrolepis*, 75%, $n = 3$; *T. nicefori*, 100%, $n = 1$), or four times (*T. brasiliensis*, 25%, $n = 1$; *T. macrolepis*, 25%, $n = 1$) broader than long. This element is distinct from the parietal, broadly contacting the latter anteriorly, the prootics laterally, and the otooccipitals posteriorly. The supraoccipital provides a dorsal cover for the *recessus scalae tympani* (otic capsule) and a small medial portion of the posterior vertical semicircular canal (Figure 3c). This element does not participate in the formation of the foramen magnum and might be externally perforated by inconspicuous foramina (*T. koppesi*, 100%, $n = 1$). The medial (internal) lamina of the supraoccipital is perforated by an endolymphatic foramen (indistinct in one specimen of *T. dimidiata*, 33%) that is located dorsoposteriorly to the acoustic nerve foramina. In *T. macrolepis* (50%, $n = 1$), an additional foramen is located dorsally to the endolymphatic foramen, opening into the horizontal semicircular canal.

The prootics (Figures 1–6) are paired elements, represented by wide convex plates that compose most of the lateral walls of the otic capsule. These elements are distinct from the otooccipitals and parietal, being in broad contact with the parietal anteriorly, the supraoccipital dorsally, the otooccipitals posteriorly and ventrally, and the parabasisphenoid ventrally. The medial (internal) wall of each prootic is irregular and pierced by a pair of acoustic nerve foramina (Figure 3a). In *T. dimidiata* (33%) and one specimen of *T. joshuai* (50%), a very reduced foramen is located dorsally to the pair of acoustic nerve foramina, opening into the *cavum vestibuli*. A perilymphatic foramen is most likely absent in all species/specimens examined.

The paired otooccipitals (Figures 1–6) are smooth and wide elements that provide most of the posterior cover of the skull (both dorsally and ventrally). These elements also participate in the formation of the posterior portion of the otic capsules (Figure 3). Each otooccipital bears an elongate dorsal lamina that forms the dorsal margins of the foramen magnum, contacting the supraoccipital and prootic anteriorly. These elements also descend to form the lateral and most of the ventral limits of the foramen magnum (Figure 2b), being posteriorly perforated by the wide vagus nerve foramen that opens internally. A small foramen might be present (*T. affinis*, 100%, $n = 1$; *T. brasiliensis*, 100%, $n = 2$; *T. joshuai*, 50%, $n = 1$; *T. macrolepis*, 50%, $n = 2$) in the posterior surface of each otooccipital that opens internally, and most likely represents the hypoglossal nerve foramina. The ventral lamina of the otooccipital might bear an elevated lamina that projects posteriorly, creating a concave area for neck muscles insertion (*T. brasiliensis*, 100%, $n = 3$; *T. macrolepis*, 100%, $n = 4$). A dorsal foramen that opens internally in the posterior semicircular foramen is present exclusively in *T. affinis* (100%, n = 1) and *T. joshuai* (100%, $n = 2$).

3.1.4 | Otic capsule

The otic capsule is composed of the prootic laterally, the supraoccipital that forms the dorsal cover of the osseous labyrinth, and the otooccipital that provides a dorsal cover for the vestibular cavity and the semicircular posterior canal (Figure 3). The acoustic nerve enters the internal region of the braincase through two medial foramina (but see prootics) into the *cavum vestibuli*. The *cavum vestibuli* represents a wide medial cavity within the otic capsule, where a wide statolithic mass is always present (Figure 3b,c). The horizontal semicircular canal is reduced and dorsal to the *cavum vestibuli*, while the anterior semicircular canal is anterior and dorsomedial to the horizontal semicircular canal. The posterior semicircular canal is located dorsoposteriorly to the *cavum vestibuli*. The stapedial plate lies in the *fenestra vestibuli*, being dorsoventrally flattened, circular, and slightly movable (not co-ossified to the prootic). It extends into a long process that crosses the area between the prootic and quadrate, and is not externally visible in *T. affinis* (100%, $n = 1$), *T. macrolepis* (50%, $n = 1$), and *T. nicefori* (100%, $n = 1$).

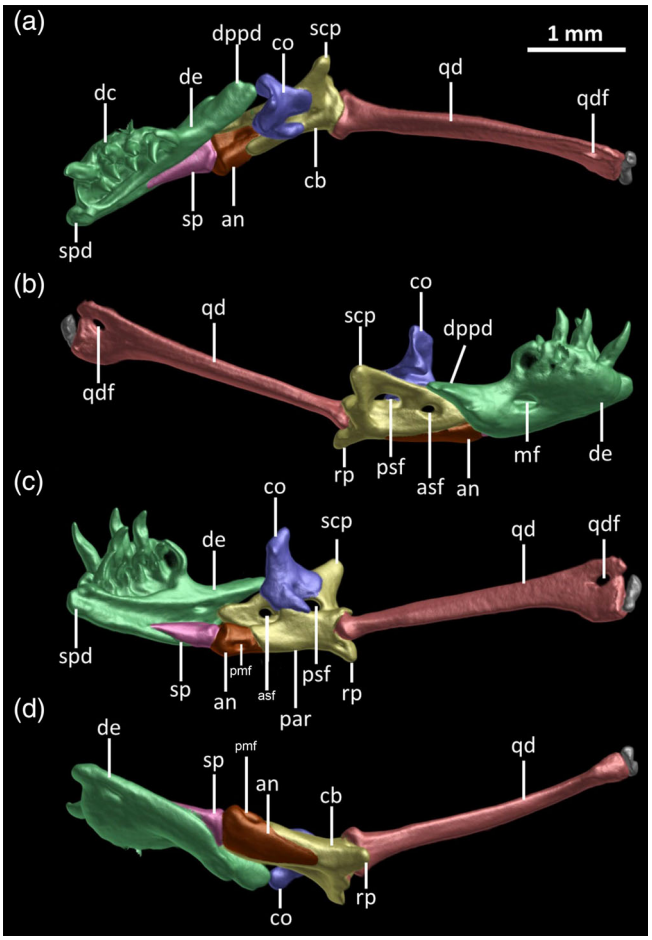

FIGURE 9 Dorsal (a), lateral (b), medial (c), and ventral (d) views on the three-dimensional reconstruction of the suspensorium (quadrate + lower jaw) of the lectotype of *Trilepida macrolepis* (ZMB 1434) based on μCT data. Different skull elements are digitally colored to improve elements visualization. an, angular; asf, anterior surangular foramen; cb, compound bone; co, coronoid; dc, dental concha; de, dentary; dppd, dorsoposterior process of dentary; mf, mental foramen; par, prearticular lamina of compound bone; pmf, posterior mylohyoid foramen; psf, posterior surangular foramen; qd, quadrate; qdf, quadrate foramen; rp, retroarticular process; scp, supracotylar process of surangular; sp, splenial; spd, symphyseal process of dentary

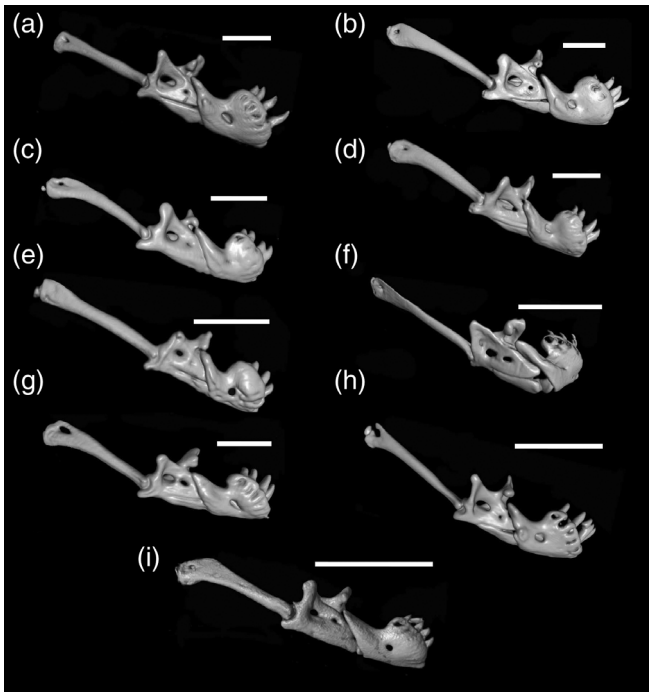

FIGURE 10 Three-dimensional reconstruction of the lower jaw of *Trilepida* spp. in lateral view. (a) *T. affinis* (BMNH 1946.1.11.16); (b) *T. brasiliensis* (RBINS 2049.12594); (c) *T. dimidiata* (MZUSP 10120); (d) *T. fuliginosa* (MNRJ 19223); (e) *T. jani* (LZV 778S); (f) *T. joshuai* (NHMW 38424.2); (g) *T. koppesi* (MNRJ 24716); (h) *T. macrolepis* (ZMB 5294); and (i) *T. nicefori* (MNHN 1900.151). Scale bars = 1 mm

3.2 | Suspensorium and mandible

In all *Trilepida* spp., the lower jaw is suspended from the skull by a pair of quadrates, which are connected to the skull by a series of muscles, ligaments and cartilages (Kley, 2006; Martins, Passos, et al., 2019) (Figures 1–3, 5–7, and 9–11). The quadrate is a long and rod-like element that ranges from 32 to 45% of the skull length, while each mandibular ramus represents 33 to 46% of the skull length, therefore being slightly longer than the quadrate (see Table 3).

The quadrate (Figures 1–5, 9, and 10) is connected to the skull at the level of the otic capsule, longitudinally to the skull, and at the level of the posterior limit of the prootics, distally articulating with the lower jaw to form the quadratomandibular joint. This bone is wide and laterally compressed at the articulation with the otic region, without any visible posterior process. At this region, it is usually perforated by a foramen (absent exclusively in one specimen of *T. koppesi*, 25% and on one side of *T. macrolepis*, 25%, $n = 1$) that is approximately ellipsoidal or rounded (Figures 1b, 5, and 10). Additionally, the proximal head of the quadrate is always associated to a cartilage that articulates with the stilohyal cartilage (most of the time visible only in cleared and stained specimens), although it is not visible in cleared and stained specimens of *T. joshuai* (100%, $n = 1$) or *T. macrolepis* (100%, $n = 1$). A stapedial cartilage was indistinct in all analyzed cleared and stained specimens/species (but see the Material Examined section in the Appendix).

The proximal head of the quadrate is slightly larger (*T. affinis*, 100%, $n = 1$; *T. brasiliensis*, 67%, $n = 2$; *T. fuliginosa*, 50%, $n = 1$; *T. jani*, 100%, $n = 3$; *T. koppesi*, 100%, $n = 4$; *T. macrolepis*, 100%, $n = 4$; *T. nicefori*, 100%,

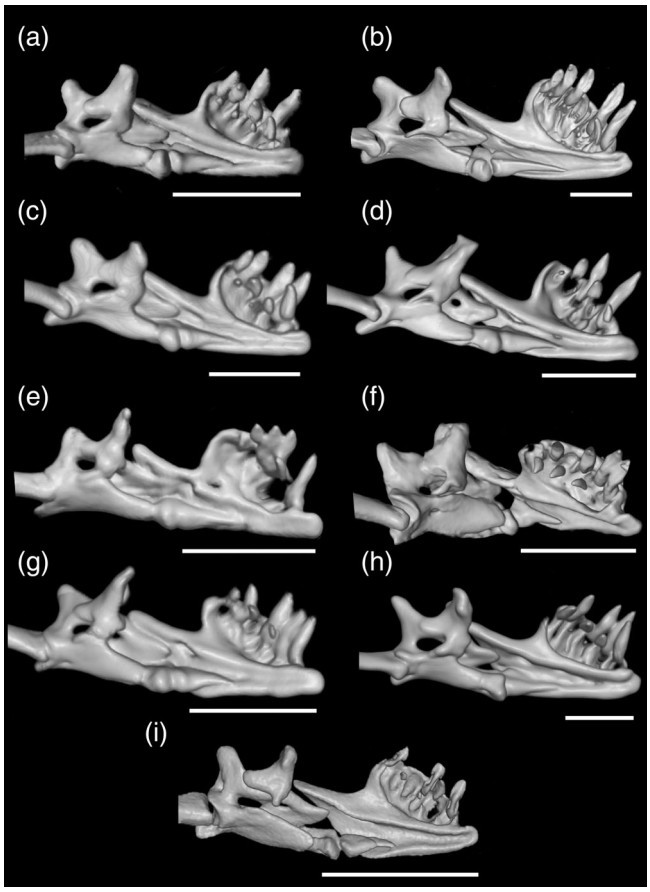

FIGURE 11 Three-dimensional reconstruction of the mandible of *Trilepida* spp. in medial view. (a) *T. affinis* (BMNH 1946.1.11.16); (b) *T. brasiliensis* (RBINS 2049.12594); (c) *T. dimidiata* (MZUSP 10120); (d) *T. fuliginosa* (MNRJ 19221); (e) *T. jani* (LZV 778S); (f) *T. joshuai* (NHMW 38424.2); (g) *T. koppesi* (MNRJ 24716); (h) *T. macrolepis* (ZMB 1434); and (i) *T. nicefori* (MNHN 1900.151). Scale bars = 1 mm

$n = 1$), about twice as large (*T. brasiliensis*, 33%, $n = 1$; *T. dimidiata*, 33%, $n = 1$; *T. fuliginosa*, 50%, $n = 1$; *T. joshuai*, 100%, $n = 1$) or three times (*T. dimidiata*, 67%, $n = 2$) larger than its distal epiphysis. This bone distally twists along its own axis, becoming progressively slenderer and angling medially toward its distal head. A foramen at the dorsoanterior face of the quadrate is indistinct/absent in all analyzed specimens/species. In one specimen of *T. fuliginosa* (50%, $n = 1$), the quadrate is perforated by a small foramen in its medial anterior lamina.

The mandible (Figures 2–3, 5, 7, and 9–11) is subterminal, short (see Table 3), paired, and composed of the dentary, splenial, angular, coronoid, and compound bone. The dentary is composed of four distinguishable regions (sensu Kley, 2006): (a) dental concha, (b) symphyseal process, (c) body of dentary, and (d) dorsoposterior process. The dental concha is wide and resembles a shallow ellipsoidal bowl with prominent convex surface in dorsal and lateral views. *Trilepida* spp. exhibit a series of 5 to 6 slightly medially curved teeth (see Table 3) with pleurodont implantation lacking a medial support. The teeth are ankylosed to the inner surface of the anterolateral margin of the dental concha. The symphyseal process of the dentary represents a reduced anteromedial projection of the body of dentary, projecting beyond the anterior limit of the dental concha. The symphyseal process also covers the dorsal, lateral, and ventral portions of Meckel's cartilage, which in turn finds its anterior limit at the level of the anterior tip of this process (*T. brasiliensis*, 50%, $n = 1$; *T. fuliginosa*, 100%, $n = 1$; *T. koppesi*, 33%, $n = 1$; *T. macrolepis*, 100%, $n = 1$), at half its extension (*T. dimidiata*, 100%, $n = 1$; *T. jani*, 50%, $n = 1$), or at its posterior region (*T. brasiliensis*, 50%, $n = 1$; *T. jani*, 50%, $n = 1$; *T. koppesi*, 67%, $n = 2$). The body of dentary is triangular-shaped and located ventral to the dental concha, being notched by Meckel's groove, that extends toward the ventromedial region of the dentary, and accommodates the slender and flexible string-like Meckel's cartilage. This cartilage is visible exclusively in cleared and stained specimens. At the tip of the dentary, the medially curved symphyseal process closes it. Posteriorly, the Meckel's cartilage is totally encircled by the compound bone. A wide mental foramen is located at the lateral surface of the body of dentary, with variable inter- and intraspecific position: it might be located below the level of the anteriormost tooth or posterior to the last tooth (see Table 3). In one specimen of *T. joshuai* (50%), a small additional foramen is located anterior to the mental foramen, below the level of the fourth tooth. The posteromedial portion of the body of dentary supports the anterior process of the splenial, covering it almost completely or completely (but see splenial variation) in lateral view. The dorsoposterior process of dentary is a long and medially oriented process that projects toward the dorsal process of the coronoid, reaching the level of the coronoid anterior limit, except in one specimen of *T. brasiliensis* (25%). An inconspicuous bony elevation is present at the lateroposterior portion of the dorsoposterior process in all species of *Trilepida*, although in *T. affinis* (100%, $n = 1$) this process is evident and most likely serves for the attachment of the *Musculus cervicomandibularis* (but see Martins, Passos, et al., 2019).

The splenial (Figures 2–3 and 9–11) is the smallest bone in the lower jaw, being approximately conical in shape and tapering anteriorly to fit below the Meckel's cartilage. A small posterior portion of this bone is always visible in lateral view (Figures 10 and 11), being connected to the medial surface of the body of dentary, leading to a functional unit capable of rotational movement. It contacts the angular posteriorly, while anteriorly it

TABLE 3 Quantitative and qualitative variation of the suspensorium and lower jaw for species of *Trilepida*. (1) Proportion of mandible length in relation to skull length; (2) proportion of quadrate length in relation to mandible length; (3) Proportion of quadrate length in relation to skull length; (4) number of teeth in dentary; (5) position of mental foramen in relation to dentary teeth; (6) anteriormost limit of splenial in relation to dentary teeth. The numbers in parentheses represent the numbers of specimens examined, except when in formula: [mean ± standard deviation (interval) number of specimens sampled]

Species	1	2	3	4	5	6
T. affinis	33 (1)	1.2 (1)	41.1 (1)	6	Posterior to sixth	Third
T. brasiliensis	39.9–43.4 (2)	1.1–1.2 (2)	32–39 (2)	6 (4)	Fifth–sixth (1) or posterior to sixth (2)	Third (2) or fourth (2)
T. dimidiata	45.6 (1)	1.3 (1)	36.1 (1)	5 (1)–6 (2)	Posterior to fifth (2) or sixth (1)	Third (2) or fourth (1)
T. fuliginosa	46.1 (1)	1.2 (1)	39.4 (1)	6 (3)	Fifth (2) or posterior to sixth (1)	Third (1) or fourth (2)
T. jani	43–45.7 (2)	1.2 ± 0.1 (1.1–1.3) 2	33.6–42.7 (2)	5 (2)	Third (1); fourth (1) posterior to fifth (1)	Third (2)
T. joshuai	40 (1)	0.8 (1)	52.2 (1)	6 (2)	Fourth (2)	Third (2) or sixth (2)
T. koppesi	40.6–46 (3)	1.2 ± 0.2 (1–1.4) 3	41.4–41.7 (2)	5 (2)–6 (2)	Third–fourth (1); fifth–sixth (1); sixth (1)	Third (1), fourth (1) or fifth (1)
T. macrolepis	37.8–42.4 (3)	0.9 ± 0.1 (0.8–1) 2	43.9–45 (2)	5 (2)–6 (2)	Posterior to last tooth (4)	Fourth (1) or fifth (2)
T. nicefori	38.6 (1)	1 (1)	39.7 (1)	6 (1)	Fifth–sixth (1)	Sixth (1)

tapers reaching the level of the last (fifth or sixth tooth) or even the third tooth (Figures 9 and 11; see Table 3). An anterior mylohyoid foramen is absent.

The angular (Figures 2–3, 5, and 9–11) resembles the splenial in shape, although it is stouter than the former. The cotylar head of the angular is convex and larger than the condylar head. The cotylar head of the angular is medially exposed. The posterior mylohyoid foramen is positioned on the ventral surface of the angular bone. The angular tapers posteriorly, reaching the level of the posterior surangular foramen.

The compound bone (Figures 2–3, 5, 7, and 9–11) represents the fusion of the articular, prearticular, and surangular. The surangular and prearticular are distinguishable by a medial separation throughout their medial contact, both fused to the articular posteriorly, which represents the widest region of the compound bone. In lateral view, the anterior process of the surangular is partially occluded by the dorsoposterior process of the dentary. The posterior edge of the surangular supports the surangular process of the coronoid through a dorsal enlargement (Figures 9 and 11). This lamina is also pierced by an anterior and a posterior foramen, which vary in terms of position and size. The posterior foramen is usually larger than the anterior, being located anterior to the articular lamina of the compound bone. The anterior foramen is reduced, located below the level of the coronoid and approximately oval or ellipsoidal. Both foramina might rarely be merged into a single foramen in a few specimens (*T. dimidiata*, 63%, $n = 2$; *T. fuliginosa*, 33%, $n = 1$; and *T. koppesi*, 25%, $n = 1$), even though this condition might vary bilaterally. The surangular lamina also expands dorsally to form the supracotylar process of the surangular, which is usually concave posteriorly (in lateral view) and projects dorsoposteriorly.

The prearticular lamina of the compound bone is mostly visible in medial view, tapering as it expands anteriorly (except for one specimen of *T. joshuai*, 50%), but not reaching the anterior limit of the surangular lamina. It also develops dorsally into a coronoid process that supports the coronoid.

The quadratomandibular joint is formed at the concavity located at the articular region of the compound bone. *Trilepida nicefori* (100%, $n = 1$) exhibits a foramen at this region that connects to the posterior surangular foramen (Figure 11i). The retroarticular process represents a short posteroventral elongation of the articular lamina. In lateral view, this process projects posterior to the level of the supracotylar process of the compound

Species	Anteriormost hyoid limit	Posteriormost hyoid limit	Hyoid extension	Cornua/lingual process relation
T. affinis	12 (1)	18 (1)	6 (1)	?
T. brasiliensis	10 (1)	17 (1)	7 (1)	1.4 (1)
T. dimidiata	13 (1)	21 (1)	8 (1)	2.6 (1)
T. fuliginosa	?	?	?	2.8 (1)
T. jani	9 (1)	16 (1)	7 (1)	2.8 (1)
T. joshuai	?	?	?	2.6 (1)
T. koppesi	?	?	?	1.8 (1)
T. macrolepis	12–15 (5)	17–22 (5)	7 (5)	3.7 (1)

TABLE 4 Summarized quantitative data in the hyoid variation of cleared and stained and X-rayed specimens for species of *Trilepida*. Anteriormost and posteriormost areas of hyoid are considered in relation to the pre-cloacal vertebrae. The numbers in parentheses represent the numbers of specimens examined

bone and is pierced posteriorly by a wide foramen. The foramen for the *chorda tympani* of the hyomandibular ramus of the facial nerve (VII) pierces the ventral portion of the articular. In *T. joshuai* (50%, $n = 1$), this foramen is wide (Figure 11f).

The coronoid (Figures 2–3, 5, and 9–11) is complex in shape, located dorsomedially to the compound bone and consists of a dorsal process, a midposterior surangular process, and a ventrolateral prearticular process. It lies horizontally along the broad dorsal support of the surangular lamina of the compound bone. Its dorsal process might be short and spoon-shaped (*T. affinis*, 100%, $n = 1$; *T. brasiliensis*, 100%, $n = 4$; *T. dimidiata*, 67%, $n = 2$; *T. fuliginosa*, 67%, $n = 2$; *T. jani*, 100%, $n = 3$; *T. joshuai*, 100%, $n = 2$; *T. koppesi*, 100%, $n = 4$; *T. macrolepis*, 75%, $n = 3$) or single and tapered dorsally (*T. fuliginosa*, 33%, $n = 1$). In all specimens of *T. macrolepis* ($n = 3$), the dorsal process projects into three short processes: a lateral, a medial and a dorsal (Figures 9, 10h, and 11h). The anterior concave surface of the dorsal process of the coronoid is usually anteriorly oriented, but it might twist laterally and be visible in lateral view (*T. jani* 33%, $n = 1$; *T. joshuai*, 100%, $n = 2$; Figure 10f). When spoon-shaped, the medial or lateral portions might be more expanded anteriorly or equally projected, and might vary intraspecifically, as follows: lateral portion projecting more anteriorly than medial portion (*T. affinis*, 100%, $n = 1$; *T. joshuai*, 50%, $n = 2$), medial portion projecting more anteriorly than lateral portion (*T. dimidiata*, 50%, $n = 1$; *T. fuliginosa*, 50%, $n = 1$; *T. joshuai*, 50% $n = 1$; *T. koppesi*, 50%, $n = 2$; *T. macrolepis*, 50%, $n = 1$), or medial and lateral portions equally or almost equally projected (*T. dimidiata*, 50%, $n = 1$; *T. koppesi*, 50%, $n = 2$; *T. macrolepis*, 50%, $n = 1$). The prearticular process of the coronoid develops a thin ventroposterior process that is in contact with the prearticular lamina (Figure 11, except 11i). In *T. nicefori*, this process is reduced and does not contact the compound bone ventrally (Figure 11i). The surangular process of the coronoid rests on the medial face of the compound bone surangular lamina. Both the surangular and prearticular processes of the coronoid form the posterior surangular foramen, providing a tight connection between the coronoid and the compound bone.

3.3 | Hyoid

The hyoid is Y-shaped and ossified in all species of *Trilepida*, being located in the first third of the trunk, between the 9th and 22nd vertebrae (but see variation in Table 4). It is composed of the lingual process and the paired cornua, which are oriented posteriorly and extend over about 6 to 7 vertebrae. The cornua are always longer than the lingual process, and might be slightly longer (*T. brasiliensis*, 100%, $n = 1$; *T. koppesi*, 100%, $n = 1$), twice as long (*T. dimidiata*, 100%, $n = 1$; *T. fuliginosa*, 100%, $n = 1$; *T. jani*, 100%, $n = 1$; *T. joshuai*, 100%, $n = 1$), or even almost four times longer (*T. macrolepis*, 100%, $n = 1$) than the lingual process (but see Table 4 for detailed data and variation).

3.4 | Larynx, glottis, and trachea

The larynx is a prominent structure located at the mouth floor, adjacent to the dental concha, and composed of the paired arytenoid cartilages and the cricoid cartilage (Figure 12). While the arytenoid cartilages are located dorsoanteriorly in the larynx and are fused posteriorly (Figure 12c) except in one specimen of *T. koppesi* (33%), the cricoid is Y-shaped and rests on the mouth floor, ventrally to the arytenoids. The arytenoid cartilages vary inter- and intraspecifically in terms of their shape and lateral edges (Figure 12d). They are usually subtriangular with irregular edges but might be semicircular with regular edges in *T. jani* (100%, $n = 2$; Figure 12d). A dorsal fold in the arytenoid cartilages is usually present, but it

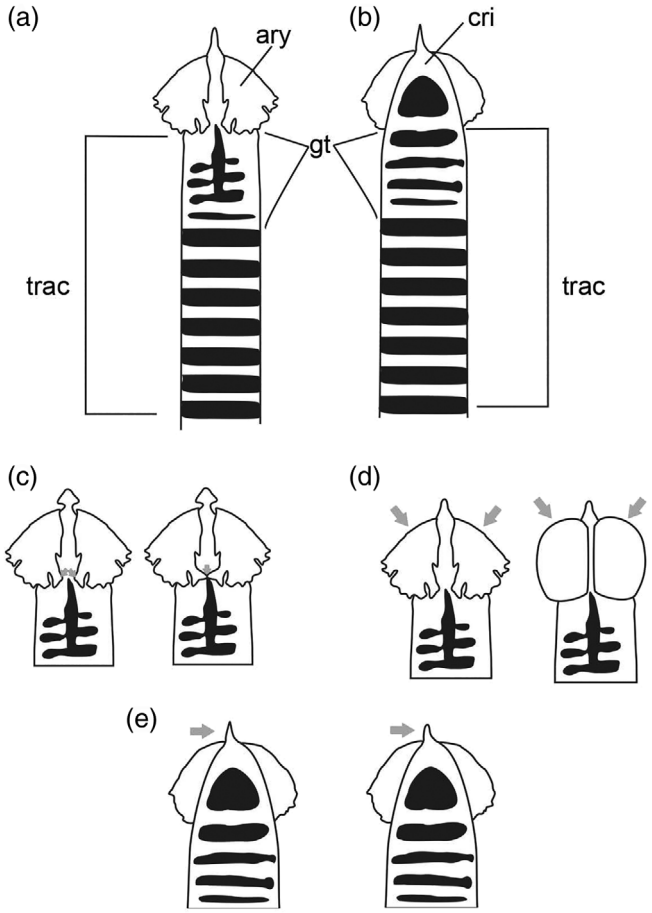

FIGURE 12 General schematic view of the larynx, glottal tube and trachea in dorsal (a) and ventral (b) views. (c) Dorsal view of larynx illustrating the posterior unfused arytenoid cartilages (left) and fused cartilages (right). (d) Dorsal view of larynx illustrating semi-triangular arytenoid cartilages with irregular edges (left) and semicircular arytenoid cartilages with regular edges (right). (e) Ventral view of larynx illustrating a tapered distal limit of cricoid (left) or rounded distal limit of cricoid (right). ary, arytenoid cartilages; cri, cricoid cartilages; gt, glottal tube; trac, trachea

varies intraspecifically in *T. koppesi*, being present in two specimens (67%). The anterior process of the cricoid (Figure 12e) is thin and anteriorly tapered (*T. brasiliensis*, 50%, $n = 1$; *T. dimidiata*, 100%, $n = 1$; *T. fuliginosa*, 100%, $n = 1$; *T. koppesi*, 100%, $n = 3$) or rounded (*T. brasiliensis*, 50%, $n = 1$; *T. jani*, 100%, $n = 2$; *T. joshuai*, 100%, $n = 1$; *T. macrolepis*, 100%, $n = 1$).

The glottis (Figure 12) represents a longitudinal slit extending from the anteriormost limit of the arytenoid cartilages to the mouth floor, and posteriorly to the glottal tube. The glottal tube represents the anteriormost portion of the trachea, posterior to the arytenoid cartilages, and is composed of a posterior extension of the cricoid cartilages and a few interconnected cartilaginous rings that vary from no interconnected rings to 19 interconnected rings (see Table 5).

The trachea (Figure 12) extends from the posterior limit of the larynx to the anterior limit of the right lung. In all analyzed species/specimens, the rings are type I and C-shaped (sensu Wallach, 2008). The real number of rings (based on counts made in specimens) vary from 121 in *T. brasiliensis* to 228 in *T. koppesi* (see Table 5). For specimens where comparisons were possible, we compared the real number of rings with estimated number of rings (considering a segment of 1 mm; see Wallach, 1998b). The estimated number of tracheal rings versus the real number of rings is usually very discrepant as of more than 62% or less than 42% (see Table 5).

We identified three types of rings considering their width: thin, moderate, and wide (sensu Wallach, 2008b), each of which might vary intraspecifically (see Table 5). Wide rings (at least three times larger) with narrow interspaces are present in *T. fuliginosa* (100%, $n = 1$) and *T. jani* (100%, $n = 2$). Moderate rings were found in specimens of *T. brasiliensis* (100%, $n = 2$), *T. dimidiata* (100%, $n = 1$), *T. joshuai* (100%, $n = 1$), and *T. koppesi* (100%, $n = 3$). Thin rings that are narrower than the interspaces were found exclusively in *T. macrolepis* (100%, $n = 1$).

3.5 | Postcranial osteology

3.5.1 | Cervical vertebrae

The atlas (Figures 4–6 and 13) is roughly rounded, lacking a neural spine and ribs, and is composed of the paired neural arches and the ventral intercentrum I. The neural arches are dorsoventrally flattened elements that are not in contact with each other dorsally or ventrally and surround the semicircular neural canal (Figure 13a–e). *T. nicefori* represents the only species with the absence of an intercentrum I, allowing the neural arches to contact each other ventrally. Each neural arch expands anteriorly and posteriorly in its dorsal region, also enlarging midventrally to form articular facets (Figure 13a,d), which are covered by cartilage and articulate with the occipital condyle of the skull. In *T. dimidiata* (33%) and one specimen of *T. joshuai* (50%), the neural arches are pierced by an anteroventral foramen that is not visible in other species/specimens.

The intercentrum I is a reduced element positioned midventrally to the neural arches, and not fused to them (Figure 13a,c–e). It is approximately rectangular with a ventral tapered projection (Figure 13a). In *T. brasiliensis*, the anterior facet of the intercentrum I is pierced by a reduced foramen that leads to a dorsal duct that runs along this element. This foramen is indistinct or absent in the other congeners.

The axis (Figures 4–6, and 13f–j) articulates with the posterior face of the atlas, being composed of a centrum,

TABLE 5 Quantitative variation in the larynx and trachea for species of *Trilepida*. (1) Number of rings in glottal tube; (2) tracheal ring/interspace ratio; (3) total number of rings in trachea; (4) estimated number of tracheal rings; (5) estimated/real number of tracheal ring ratio; (6) number of rings in 10% of snout-vent length. The numbers in parentheses represent the numbers of specimens examined, except when in formula: [mean ± standard deviation (interval) number of specimens sampled]

Species	1	2	3	4	5	6
T. brasiliensis	5.5 ± 7.7 (0–11) 2	2.4 ± 0.2 (2.1–2.5) 2	161	125	77%	80
T. dimidiata	9 (1)	1.9 (1)	?	?	?	90
T. fuliginosa	13 (1)	3.1 (1)	?	?	?	40
T. jani	11 (2)	3.6 ± 0.9 (3–4.3) 2	143	149	104%	40
T. joshuai	11 (1)	2.6 (1)	?	?	?	64
T. koppesi	15 ± 3.4 (13–19) 3	2.5 ± 0.3 (2.1–2.8) 3	228	384	168%	22
T. macrolepis	0 (1)	0.8	?	?	?	44

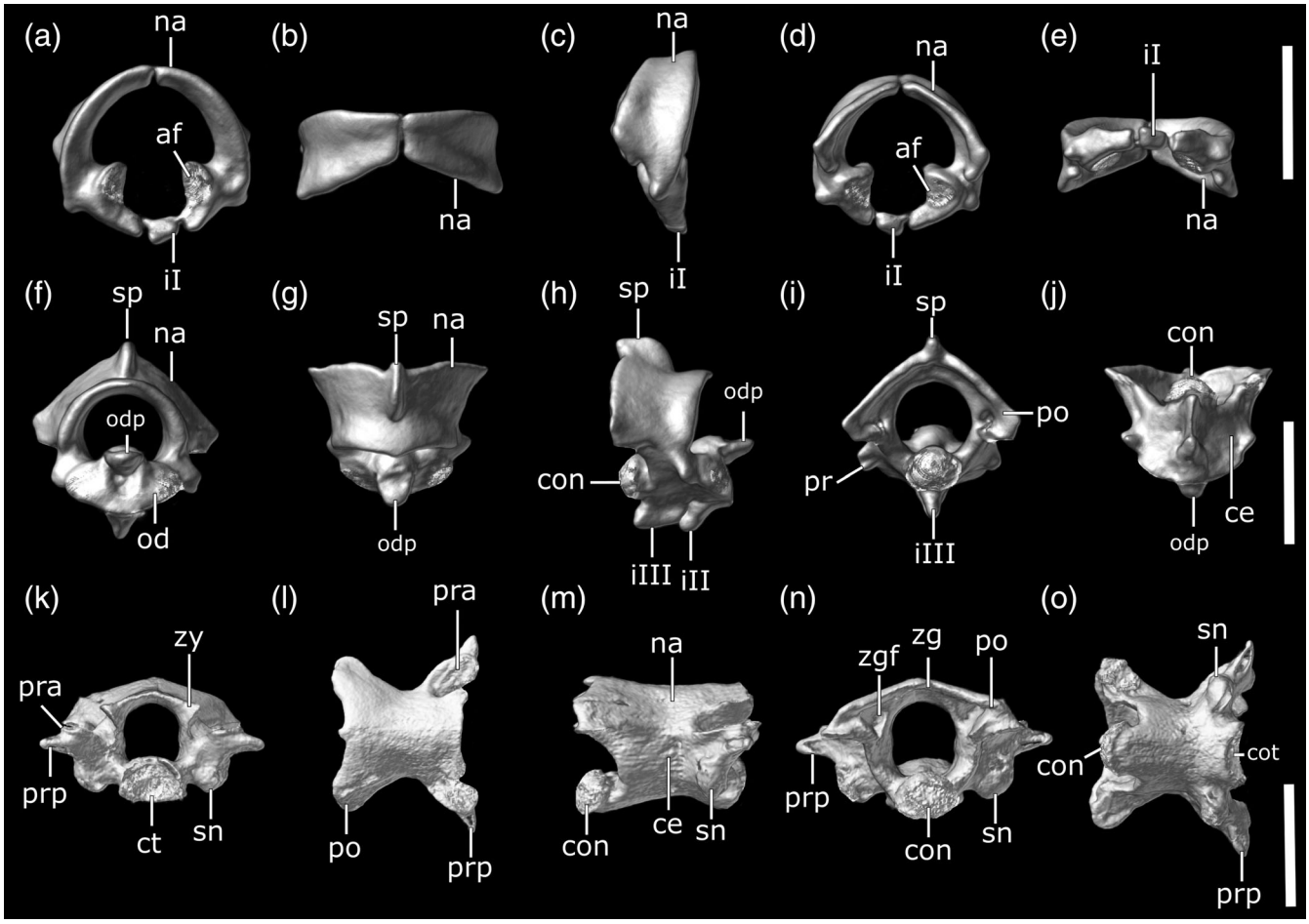

FIGURE 13 Three-dimensional reconstruction of the atlas (a–e), axis (f–j) and midtrunk (k–o) vertebrae of *Trilepida macrolepis* (a–j, ZMB 1434) and the holotype of *T. affinis* (k–o, BMNH 1946.1.11.16) in anterior (a,f,k), dorsal (b,g,l), lateral (c,h,m), posterior (d,i,n), and ventral (e,j,o) views. af, articular facet; ce, centrum; con, condyle; cot, cotyle; iI, intercentrum I; iII, intercentrum II; iIII, intercentrum III; na, neural arches; od, odontoid; odp, odontoid process; po, postzygapophysis; pr, prezygapophysis; pra, prezygapophyseal articular facet; prp, prezygapophyseal accessory process; sn, synapophyses; sp, spinal process; zg, zygantrum; zgf, zygantral articular facet; zy, zygosphene. Scale bars = 1 mm

moderate neural arches, a reduced spinal process, an odontoid process, a dorsoanterior process of the odontoid, a condyle and the intercentra II and III. As with the atlas, this vertebra has no vestiges of ribs. The axis spinal process—very inconspicuous in *T. affinis* (100%, $n = 1$)—is reduced, curved posteriorly with a rounded tip, barely

projecting beyond the posterior limits of the neural arches (Figure 13f–i). The neural canal is always oval, and the odontoid is an osseous process attached to the anteroventral surface of the neural arches (Figure 13f). A dorsoanterior projection from the odontoid is visible anteriorly, tapering anteriorly, and ending in a rounded distal limit (Figure 13f,h). A well-developed keel extends over the ventral lamina of the neural canal until reaching the condyle. The centrum of the axis is pierced by two small foramina on each side, although these foramina are indistinct in *T. dimidiata* (33%, $n = 1$), *T. joshuai* (50%, $n = 1$), *T. macrolepis* (33%, $n = 1$), and *T. nicefori* (100%, $n = 1$). The ventralmost foramen is situated dorsal to the intercentra II and III, while the second is located dorsally to the former. Short posterolateral projections from the centrum are present in all analyzed specimens.

The intercentra II and III are laterally compressed and might vary in terms of their fusion or shape (Figures 5 and 13h). When fused (*T. jani*, 50%, $n = 2$; *T. nicefori*, 100%, $n = 1$), both elements are keel-shaped in lateral view. When distinct as two elements, the intercentrum II is fused to the odontoid and keeled (*T. fuliginosa*, 67%, $n = 2$; *T. jani*, 50%, $n = 1$), rounded (*T. brasiliensis*, 80%, $n = 4$; *T. dimidiata*, 100%, $n = 2$; *T. fuliginosa*, 33%, $n = 1$; *T. jani*, 50%, $n = 1$; *T. koppesi*, 50%, $n = 1$; *T. macrolepis*, 50%, $n = 1$), pointed (*T. brasiliensis*, 20%, $n = 1$; *T. joshuai*, 100%, $n = 1$; *T. macrolepis*, 50%, $n = 1$), or truncate (*T. koppesi*, 50%, $n = 1$). The intercentrum III when distinct from the intercentrum II is fused to the axis ventral body region and keeled (*T. brasiliensis*, 67%, $n = 2$; *T. fuliginosa*, 50%, $n = 1$; *T. koppesi*, 50%, $n = 1$), rounded (*T. dimidiata*, 100%, $n = 2$; *T. fuliginosa*, 50%, $n = 1$; *T. jani*, 100%, $n = 1$; *T. joshuai*, 100%, $n = 1$; *T. macrolepis*, 50%, $n = 1$), pointed (*T. brasiliensis*, 33%, $n = 1$), or truncate (*T. koppesi*, 50%).

3.5.2 | Trunk vertebrae

The species of *Trilepida* analyzed herein exhibit a total number of 135 to 219 trunk vertebrae (Figure 13; but see Table 6) that are dorsoventrally depressed, with depressed neural arches lacking neural spines, all bearing a pair of ribs articulated to their ventrolateral surface. The first trunk vertebrae (posterior to the cervical vertebrae) do not bear conspicuous zygosphenes, which are gradually perceptible posteriorly from the posterior 1/3 of the vertebral column. In dorsal view, the anterior limit of the zygosphene is convex with tapered lateral limits that curve medially. The prezygapophyses are visible in anterior view and represent lateral projections that bear prezygapophyseal articular facets that are oval or ellipsoidal (Figure 13k). The prezygapophyseal accessory processes vary intraspecifically in terms of their shape from thin and long (*T. brasiliensis*, 100%, $n = 2$; *T. dimidiata*, 100%, $n = 1$; *T. fuliginosa*, 100%, $n = 2$; *T. jani*, 100%, $n = 1$; *T. koppesi*, 100%, $n = 3$; *T. macrolepis*, 100%, $n = 1$), to thin and short, with their distal tip being blunt (*T. joshuai*, 100%, $n = 1$). The cotyle is a wide oval concave articular surface located anterior to the *centrum*, with absent/indistinct paracotylar foramina.

The vertebral *centrum* is narrow, with the synapophyses emerging laterally at its anteroventral region (Figure 13m–n). The synapophyses form a single facet without any clear distinction between the diapophyseal and parapophyseal areas. The lateral foramina and hemal keel are absent, and a subcentral foramen is absent in *T. brasiliensis* (100%, $n = 2$), *T. jani* (100%, $n = 2$), *T. joshuai* (100%, $n = 1$), and *T. macrolepis* (100%, $n = 1$).

The anterior trunk vertebrae might or might not exhibit undeveloped hypapophyses, which are always restricted to the 10 anteriormost trunk vertebrae even though this number might vary inter- and intraspecifically (see Table 6). An anteroposterior variation in trunk vertebrae was noted mostly regarding the level of zygosphene development and for the presence of the accessory prezygapophyseal processes, which are undeveloped or absent in the anteriormost vertebrae.

In the posterior region of the trunk vertebrae, the zygantrum forms the posterior roof for the neural canal (Figure 13n). The zygantral articular facets are V-shaped and present in the internal lateral limit of the neural canal (Figure 13n). The postzygapophyses are short and triangular and laterally emerge from the neural arch (Figure 13n). The condyle is wide (Figure 13m,n), oval, and articulates with the cotyle of the subsequent vertebrae.

3.5.3 | Ribs

The ribs are elongated and medially oriented elements that articulate to the synapophyses of their respective vertebrae. The proximal head of the rib is covered by a cartilaginous layer, articulating via a single facet of the vertebrae. A tuberculiform process is present, and a single foramen is located at the ventromedial lamina of the rib head. No lateral foramina are present. Each integumentary facet is associated with a W-shaped costal cartilage (visible in cleared and stained specimens). The proximal limit of the costal cartilage does not exhibit an osseous projection that surrounds the former. The proximal region of each cartilage slightly tapers distally, projecting laterally to distally form the body and the lateral extensions of this structure. The lateral extensions of the cartilages are proximally oriented and slightly bend

TABLE 6 Quantitative variation in trunk, cloacal, and caudal vertebrae for species of *Trilepida*. (1) Total number of trunk vertebrae; (2) total number of trunk vertebrae with dorsoposterior projection; (3) number of trunk vertebrae bearing hypapophyses; (4) number of cloacal vertebrae; (5) number of caudal vertebrae; (6) number of fused caudal vertebrae. The numbers in parentheses represent the numbers of specimens examined, except when in formula: [mean ± standard deviation (interval) number of specimens sampled]

Species	1	2	3	4	5	6
T. affinis	192 (1)	>9 (1)	2 (1)	4 (1)	21 (1)	3 (1)
T. brasiliensis	184 ± 11.2 (172–198) 8	2–12 (2)	3–4 (2)	4 (2)	18–20 (2)	2–3 (2)
T. dimidiata	180 (2)	1 (1)	1 (1)	4 (2)	17–18 (2)	3 (2)
T. fuliginosa	184.5 ± 5.3 (179–190) 4	1 (1)	8 (1)	4 (1)	22 (1)	2 (1)
T. jani	159.3 ± 5.5 (154–165) 3	1 (2)	5–7 (2)	3–4 (2)	22 (1)	2 (2)
T. joshuai	158–162 (2)	>2 (1) or >7 (1)	>2 (1) or >7 (1)	3–5 (2)	17 ± 2 (15–19) 3	3 (1)
T. koppesi	173.4 ± 8 (162–185) 7	14.3 ± 22.2 (1–40) 3	1.7 ± 0.6 (1–2) 3	3.6 ± 0.6 (3–4) 3	20.3 ± 2.1 (18–21) 3	2.6 ± 0.6 (2–3) 3
T. macrolepis	207.5 ± 8 (196–219) 6	17 (1)	3–8 (2)	3.4 ± 0.5 (3–4) 5	19 (4)	3 (1)
T. nicefori	135 (1)	1 (1)	5 (1)	4 (1)	16 (1)	3 (1)

toward the rib. The axillary region of the cartilage is roughly rectangular in shape.

3.5.4 | Cloacal vertebrae

The cloacal vertebrae (Figure 14) vary from three to five in total in *Trilepida* spp. (see Table 6), being relatively more dorsoventrally compressed in comparison with the trunk vertebrae. Each cloacal vertebrae bear a pair of lymphapophyses that are fused to their ventrolateral surfaces (Figure 14a–e). The lymphapophyses develop ventrolaterally, with the dorsal element usually bending ventrally, while the ventral element bends dorsally. Each lymphapophysis bears a short and tapered costal cartilage at its distal tip. A short prezygapophyseal accessory process is also present, while the synapophyses, interzygapophyseal keel, subcentral keel, hemal keel, and subcotylar and paracotylar foramina are always absent (Figure 14a–e). In comparison to the trunk vertebrae, the cloacal vertebrae bear moderate neural arches that develop anteriorly into a short zygosphene (Figure 14a–d). Finally, the condyle of the cloacal vertebrae is considerably smaller than in the trunk vertebrae (Figure 14d).

3.5.5 | Caudal vertebrae

The caudal vertebrae (Figure 14) vary from 17 to 22 in *Trilepida* spp. (see Table 6), resembling the cloacal vertebrae in shape except for the presence of paired pleurapophyses (vs. lymphapophyses in the cloacal vertebrae; Figure 14f–j). A poorly developed zygosphene and zugantra are present in all analyzed species (Figure 14f–j). The costal cartilages are rod-shaped and associated with the distal end of the pleurapophyses. The last two or three caudal vertebrae are fused into a single unit (see Table 6). This fused unit is conical and exhibits a bifurcated posterior tip. Ventral ossified rod-like structures (= urostyle sensu List, 1966) are absent. A hemapophysis, lateral foramen, and paired subcentral foramina are absent. The prezygapophyseal articular facet is present (Figure 14g).

3.5.6 | Rudimentary pelvic and hindlimb elements

Rudimentary pelvic and hindlimb elements are present in all *Trilepida* species, being composed of the ilium, ischium, pubis, and a femur (Figures 15 and 16). These bones radiate from the acetabular region, and are covered by a massive complex of muscles, although a sacroiliac bony joint was not identified in any of the specimens. These elements are associated with a distal cartilaginous tip (visible exclusively in cleared and stained specimens). The four rudimentary elements are located ventral to the posterior trunk vertebrae or to the cloacal vertebrae and extend over three to six vertebrae (see Table 7).

The ilium is a long rod-like curved bone, oriented lateroposteriorly to the body, and represents the longest

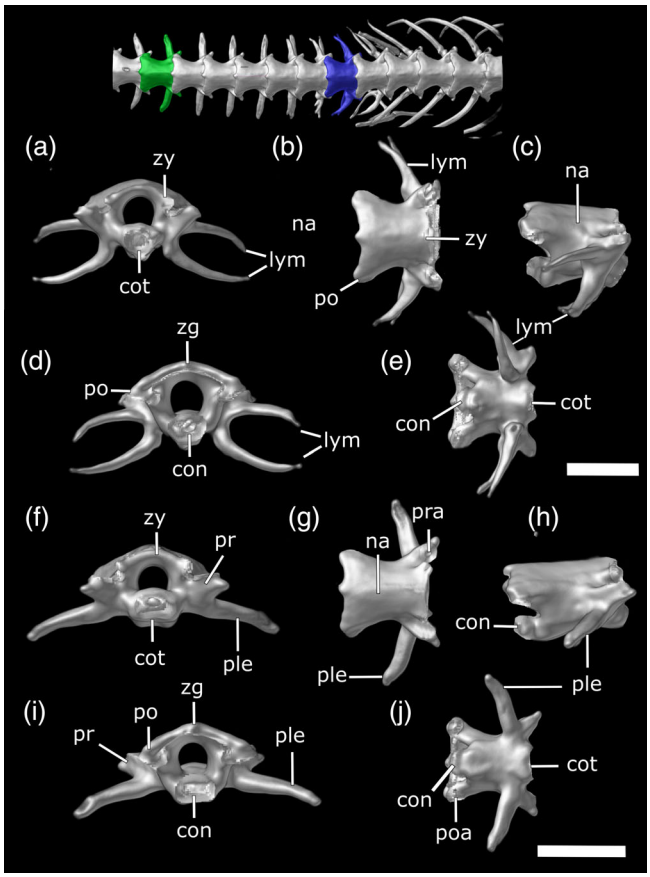

FIGURE 14 Three-dimensional reconstruction of cloacal and caudal vertebra of *Trilepida macrolepis* (ZMB 5722) in anterior (a,f), dorsal (b,g), lateral (c,h), posterior (d,i), and ventral (e,j) views. The figure above vertebrae a–j represents a dorsal view of the posterior region of the body indicating the cloacal (blue) and caudal (green) vertebra isolated and illustrated. con, condyle; cot, cotyle; lym, lymphapophyses; na, neural arches; ple, pleurapophyses; po, postzygapophysis; poa, postzygapophyseal articular facet; pr, prezygapophysis; pra, prezygapophyseal articular facet; pr, prezygapophysis; zg, zygantra; zy, zygosphene. Scale bars = 1 mm

component of the pelvic girdle. Although it does not vary much in shape, it varies in size, being long (twice as long as the ischium) or moderate (slightly longer than the ischium; see Table 7). The cartilage associated to the distal tip of the ilium might be L-shaped (Figure 16a,b,f), T-shaped (Figure 16c,g), or curved rod-shaped (Figure 16d, e,h; see Table 7 for variation). In *T. nicefori* (100%, $n = 1$), the ilium is fused to the pubis (Figure 15g).

The pubis represents the anteriormost bone of the pelvic elements, oriented at 45° medially to the body, converging to the opposite pubis but without contacting it. It is an essentially rod-like bone approximately the length of the ischium, enlarging proximally, with its distal tip bearing an elongate cartilage that might be long (longer than the pubis itself; Figure 16c), moderate (longer than half the extension of the pubis but not longer than it; Figure 16a,g,h), or short (shorter than half the pubis; Figure 16b,d–f; see Table 7).

The ischium is an elongate and curved bone, transversally oriented to the body. Exclusively in *T. brasiliensis* ($n = 1$; Figure 16a), this element bifurcates distally into a short medial portion and a long process that bears the distal cartilage, which in all specimens is a curved rod-like shaped structure.

The femur is short and stout, oriented longitudinally along the body axis. Its general shape varies both inter- and intraspecifically, being in general subquadrangular and distally bifurcate, with a claw-like cap (= femoral spur) that less commonly protrudes externally anterior to the cloaca (Figures 15a–c and 16a,c). The claw region is distinguishable from the rest by a conspicuous cartilaginous area in *T. brasiliensis* (50%, $n = 1$) or by a visible sulcus (*T. macrolepis* 20%, $n = 1$; Figure 15f). In *T. affinis* (100%, $n = 1$), *T. dimidiata* (50%, $n = 1$), and *T. joshuai* (50%, $n = 1$), the femur is divided in two distinguishable regions, with a stout proximal element and a claw-like distal element (Figures 15a–c and 16a,c). The femur is pierced by a small foramen in *T. affinis* (100%, $n = 1$), *T. dimidiata* (100%, $n = 1$), *T. joshuai* (100, $n = 1$), *T. macrolepis* (33%, $n = 1$), and *T. nicefori* (100%, $n = 1$; Figure 15).

4 | DISCUSSION

4.1 | Skull morphology in the genus *Trilepida*

Studies on the skull morphology represent one of the primary sources for obtaining data on snakes' systematics (Cundall & Irish, 2008), and have previously been applied in Leptotyphlopidae systematics and taxonomy (Koch et al., 2019; Martins, Koch, et al., 2019). The snake skull morphology also provides unique insights on the phenotypic evolution, such as functional morphology and primary homology (Cundall & Irish, 2008; Miralles et al., 2018; Rieppel, 1988). Especially for snakes, the huge divergence and specialization of the skull triggered by shifts in shape, size, and distinct levels of mobility or articulation of the bones, ensures most of the snake's evolutionary success (Cundall & Greene, 2000; Cundall & Irish, 2008; Gans, 1961). Studies on skull morphology of the fossorial snakes known as threadsnakes (= family Leptotyphlopidae) are relevant considering that this *bauplan* reflects not only their diet, but also their mode of locomotion (Wake, 1993).

All skull and lower jaw elements described herein resemble in their morphology those of the

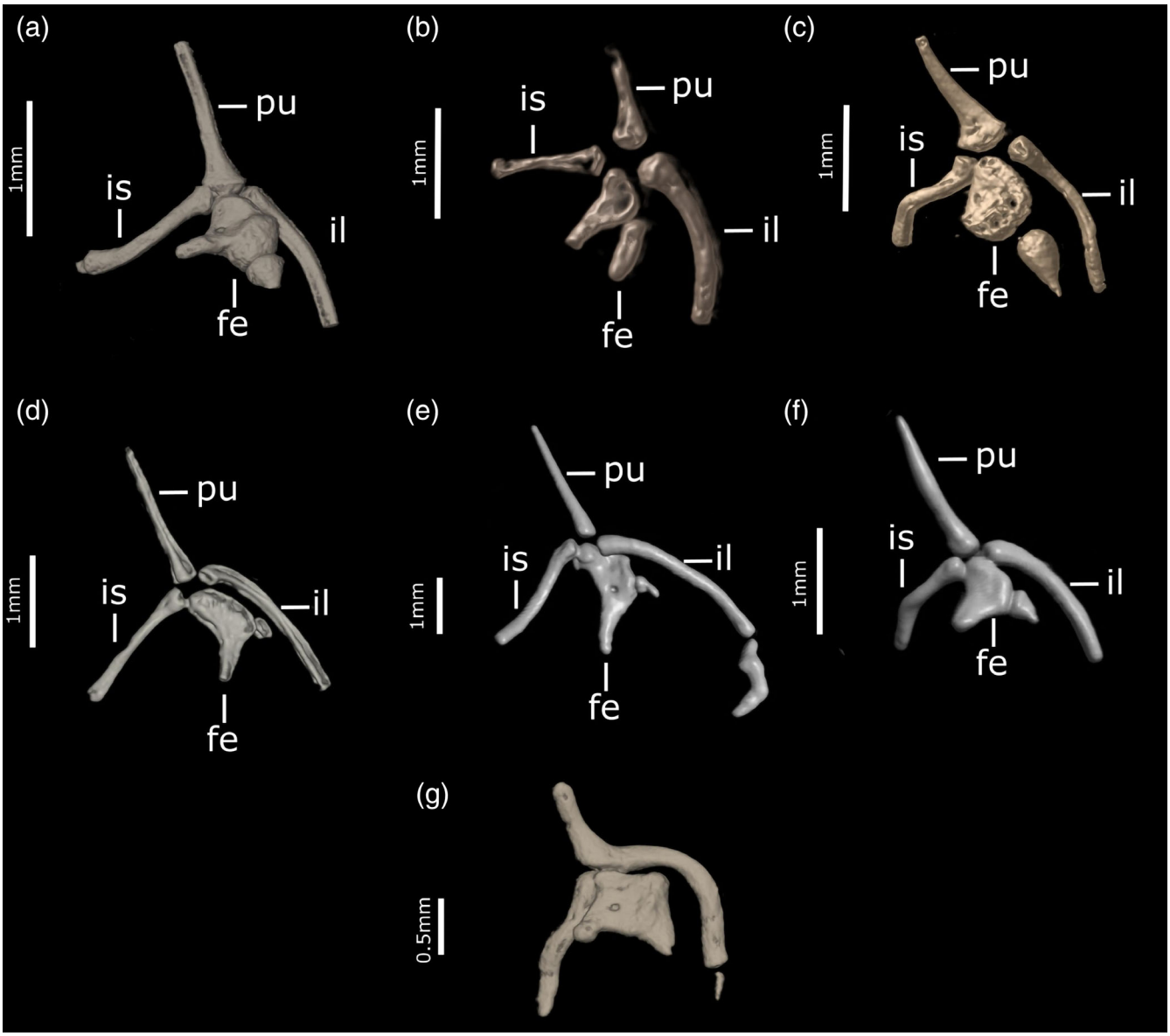

FIGURE 15 Three-dimensional reconstruction of the pelvic and hindlimb elements of *Trilepida* spp. in lateral view. (a) *T. affinis* (BMNH 1946.1.11.16); (b) *T. dimidiata* (BMNH 1994.241); (c) *T. joshuai* (NHMW 38424.2); (d) *T. macrolepis* (ZMB 1434); (e) *T. macrolepis* (ZMB 5294); (f) *T. macrolepis* (ZMB 5722); and (g) *T. nicefori* (MNHN 1900.151). fe, Femur; il, Ilium; is, Ischium; pu, Pubis

Leptotyphlopidae, especially the Epictinae (Broadley & Wallach, 2007; Brock, 1932; Koch et al., 2019; List, 1966; Pinto et al., 2015; Rieppel et al., 2009). Most skull bones exhibit a certain degree of intra- and/or interspecific variation, with elements from the basicranium and palatomaxillary complex (basioccipital, parabasisphenoid, palatines, and pterygoids), prefrontals, frontals, and vomers exhibiting the lowest degree of inter- and intraspecific variability. Most of the variability found in elements (quantitative and qualitative data) relates to foramina and the shape of skull and lower jaw elements, especially with respect to their suture and margin shapes. This apparent polymorphism has previously been reported for other Leptotyphlopidae (Koch et al., 2019; Martins, Koch, et al., 2019; Pinto et al., 2015), with variation of a few reduced foramina—mostly those of the internal surfaces of the skull—perhaps also being influenced by biases of the methods of image acquisition, as previously mentioned by a few authors (Martins, Koch, et al., 2019; Pinto et al., 2015).

The elements of the snout complex are organized in such a way that integrates elements from both the traditionally known "outer shell design" and "central rod design" (Cundall & Rossman, 1993). Although Cundall and Rossman (1993) considered that the organization of the skull elements belonging to a typical "outer shell

design" was essentially the same regardless of the variability in the skull morphology of representatives of Scolecophidia, Rieppel et al. (2009) strictly limited the standard "outer shell design" to Typhlopoidea, so that Anomalepididae and Leptotyphlopidae would exhibit functional modifications to this model. According to the data gathered herein, the nasals, premaxilla, and prefrontals act as primary receptors for the forces generated by excavation, secondarily transmitting them via the frontals dorsoposteriorly in *Trilepida* spp. Additionally, the forces are conducted ventrally from the primary receptors via the enlarged nasal septum and secondarily via the septomaxillae, until reaching the subolfactory processes of the frontals, and thus in accordance with the "central rod design" (also reported by Rieppel et al., 2009). Apparently, minor primary forces might also be laterally conducted through the dorsolateral processes of the septomaxillae to their ventral lamina and, finally transmitting the kinetic energy to the choanal processes of the palatines, which could potentially dissipate this energy to the anterior limit of the parabasisphenoid medially (present study).

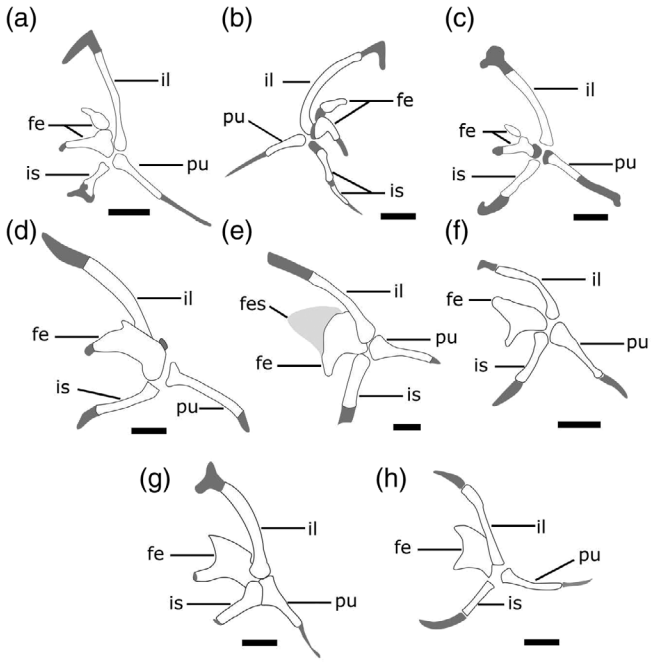

FIGURE 16 Schematic illustration of the rudimentary pelvic and hindlimb elements of cleared and stained specimens of *Trilepida* spp., with illustration of the morphological variability in the shape and size of osseous and cartilaginous elements. Gray areas represent cartilaginous (blue-stained) areas. (a) *T. brasiliensis* (UFMT 1159); (b) *T. brasiliensis* (UFMT 1163); (c) *T. dimidiata* (MZUSP 10090); (d) *T. fuliginosa* (CHUNB 40847); (e) *T. jani* (MNRJ 16990); (f) *T. joshuai* (IBSP 8919); (g) *T. koppesi* (MNRJ 24715); and (h) *T. koppesi* (CHUNB 40788); fe, femur; fes, femoral spur; il, ilium; is, ischium; pu, pubis. Scales: 0.5 mm

In all members of the genus *Trilepida*, the premaxilla represents an edentulous element that forms the anterior region of the skull, with a typical conformation of other Scolecophidia (Brock, 1932; List, 1966; Rieppel et al., 2009). Variability (inter- and intraspecific) found in the number of premaxillary foramina and in the shape of the premaxillary vomerine process has already been reported and illustrated (Koch et al., 2019; List, 1966; Pinto et al., 2015), and indicates that these conditions are highly labile among leptotyphlopids. Finally, although the size of the nasal process (when present) also varies intra- and interspecifically, this process is always inconspicuous within each considered species.

The nasals are always paired in *Trilepida* spp., contrasting with the fused pattern found in several other

TABLE 7 Quantitative and qualitative inter- and intraspecific variation of the rudimentary pelvic elements (ilium, ischium, femur and pubis) for species of *Trilepida*. (1) Anteriormost limit of rudimentary pelvic elements in relation to precloacal vertebrae; (2) posteriormost limit of rudimentary pelvic elements in relation to cloacal vertebrae; (3) extension of pelvic elements in relation to number of trunk+cloacal vertebrae; (4) shape of cartilage associated to illium; (5) size of cartilage associated to pubis; (6) ilium size. The numbers in parentheses represent the numbers of specimens examined

Species	1	2	3	4	5	6
T. affinis	2 (1)	2 (1)	4 (1)	?	?	M (1)
T. brasiliensis	2 (1)	2 (1)	4 (1)	Ls (1) or Ts (1)	L (2)	L (2)
T. dimidiata	2 (2)	2 or 3 (2)	4 or 5 (1)	Ts (1)	L (1)	M or L (2)
T. fuliginosa	2 (1)	2 (1)	4 (1)	Rs (1)	M (1)	L (1)
T. jani	3 (1)	2 (1)	5 (1)	Rs (2)	S (2)	M (1) or L (1)
T. joshuai	2 (2)	2 (2)	4 (2)	Ls (1)	M (1)	L (2)
T. koppesi	4 (1)	1 (1)	5 (1)	Ts (1) or Rs (1)	S (1) or M (1)	L (2)
T. macrolepis	1–4 (5)	1 (5)	3 (5)	Rs (1)	M	M (3) or L (1)
T. nicefori	3	3	6	?	?	L (1)

Abbreviations: L, long; Ls, L-shaped; M, moderate; Rs, rod-shaped; S, short; Ts, T-shaped.

Leptotyphlopidae (Broadley & Wallach, 2007; Brock, 1932; Fabrezi et al., 1985; List, 1966). Even though in some other leptotyphlopid species/specimens there might be a central suture that indicates an incomplete fusion of nasals (List, 1966), both nasals were conspicuously distinguishable in all specimens examined herein, in accordance with other *Trilepida* (List, 1966; Pinto et al., 2015; Salazar-Valenzuela et al., 2015).

The presence of a foramen for the *apicalis nasi* nerve formed by the lateral border of the nasal and the medial border of the prefrontal has previously been considered as exclusive to Leptotyphlopidae, while in Typhlopoidea these foramina are located at the posterior limit of the nasal dorsal lamina (Pinto et al., 2015; Rieppel et al., 2009; Salazar-Valenzuela et al., 2015). Herein, we found that the frontals might also participate in such formation in *T. nicefori*, displacing these foramina to a much more posterior region, even though it most likely represents a very uncommon pattern for the genus, and might be examined in terms of a possible intraspecific variation in the future.

The homology of the element named herein as prefrontal has been a matter of debate for "Scolecophidia" and Anomalepididae (Dunn, 1941; Dunn and Tihen, 1944; Haas, 1964, 1968; List, 1966; McDowell and Bogert, 1954). However, shape and topographical features observed in Leptotyphlopidae (Rieppel et al., 2009; present study) allows us to corroborate Haas' (1964, 1968) proposition of homologizing this element to a prefrontal. The results obtained by Martins, Passos, et al. (2019) demonstrate that—as in all snakes—the oblique eye muscles originate in the prefrontal (Romer, 1956; Underwood, 1970), as it also occurs for other members of Epictinae (Martins, Passos, et al., 2019). The variation found in the anterior lamina of the maxillary process of the prefrontal, mostly that related to the recess, is most likely associated with the inter- and intraspecific variation found in the position of the nasal gland among *Trilepida* spp. (see Martins et al., 2018).

The vomers of *Trilepida* spp. bear well-developed lateral wings and short posterior wings, exhibiting an extensive contact between these elements and the palatines. Although the vomer morphology is conserved in Leptotyphlopidae, the terminology adopted for this element is disputed in the literature. These inconsistencies have been widely discussed in Pinto et al. (2015), and our extensive data reinforce that a prevomer or any structure of this nature is not found in the genus *Trilepida*.

An ectopterygoid is absent in all species of *Trilepida* (Salazar-Valenzuela et al., 2015; Pinto et al., 2015; present study), with its absence being considered as an exclusive feature of Leptotyphlopidae and Typhlopoidea within Serpentes (McDowell, 1974). However, this element has previously been reported for Leptotyphlopidae by McDowell and Bogert (1954; *T. dimidiata*) and List (1966; *Rena maxima*) as an element fused to the posterior process of the maxilla, which was later emphasized by McDowell (2008). Although Haas (1959) confirmed the absence of an ectopterygoid in *Myriopholis macrorhyncha*, the author points out that the presence of reduced ossification incorporated in the soft palate, lateral to the internal nostril, and dorsal to the ectochoanal cartilage could represent a possible ectopterygoid or even an isolated portion of the palate. As previously mentioned by Pinto et al. (2015), the ossified element reported by Haas (1959) quite possibly represents an ossification of the hypochoanal cartilage (which we also corroborate herein). Additionally, a suture was not verified between the lateral lamina of the jaw and its posterior process in any of the specimens examined. The presence of a *Musculus pterygoideus* originating in the process of the maxilla (Martins, Passos, et al., 2019), as occurs in several Alethinophidia, reinforces the idea that this process does not represent a distinct ectopterygoid but merely a posterior elongation of the maxilla.

In all representatives of the genus *Trilepida* examined herein, as well as in other Leptotyphlopidae (Brock, 1932; Fabrezi et al., 1985; Koch et al., 2019; List, 1966; Martins, Koch, et al., 2019; Rieppel et al., 2009), a posterior orbital element (sensu Palci & Caldwell, 2013) is absent. This curved and rod-shaped element—which has for long been the subject of great debate regarding its homology—is present exclusively in Anomalepididae and Alethinophidia (Palci & Caldwell, 2013). Considering recent molecular hypotheses recovering "Scolecophidia" as paraphyletic (Miralles et al., 2018), the absence of a posterior orbital element might represent a secondary loss in the clade Leptotyphlopidae + Typhlopoidea and, therefore, a possible synapomorphy for the clade.

According to Pinto et al. (2015), the presence of a maxillary process of the palatine that is ventrally curved in its anterior portion could represent a synapomorphy of the subtribe Renina. These authors suggest this hypothesis based on the illustrations of List (1966) and from his description of *T. salgueiroi*, and this character was also found in the species examined herein. However, considering available data from Martins (2016), Koch et al. (2019), and Martins, Koch, et al. (2019), we refute this suggestion considering the well-developed maxillary process that curves and ventrally expands is also present in *Epictia*, even though it is absent in some species of *Rena*.

The parietal of *Trilepida* spp. is always fused, without any trace of a medial suture or fontanelle (List, 1966; Pinto et al., 2015; Salazar-Valenzuela et al., 2015; present

study), contrasting with other Leptotyphlopidae (mostly those from Leptotyphlopinae; List, 1966). The parietal forms—mostly with the prootics and less commonly with both prootics and parabasisphenoid—the foramen for the trigeminal nerve. We detected inter- and intraspecific variation in relation to the elements that form the trigeminal nerve foramen with the parietal, which most likely indicates that this(ese) character(s) is(are) variable among threadsnakes of the family Leptotyphlopidae. However, recent studies (see Deolindo et al., this volume; and Lira and Martins, this volume) suggest that these characters might be systematically useful in members of Typhlopidae and must be considered in future studies on scolecophidians. The posterior internal wall on each side of the parietal exhibits a well-developed lamina, herein named "internal pillar" of the parietal, which is apparently present in a few other scolecophidians (Rieppel et al., 2009), and is ventrally accompanied by the dorsal growth of the parabasisphenoid. Even though the nature of this pillar is still unknown and demands further investigations in terms of its homology, it seems to represent a medial bend of the laterally descending lamina of the parietal.

We observed variability in the basioccipital with respect to its suture shape and the presence of foramina in its dorsal (internal) surface (as mentioned above), as well as with respect to the presence of concavities for the insertion of neck muscles. These structures for the insertion of neck muscles have already been reported in the literature (Koch et al., 2019), and appear to be restricted to larger-sized individuals. In all species of *Trilepida*, the basioccipital contributes to the formation of the foramen magnum. Considering also the available literature data, this character seems to have a systematic value for Leptotyphlopidae (see Martins, Koch, et al., 2019), given that this contact appears to occur exclusively in the representatives of the subtribe Renina (*Rena* + *Trilepida*; but see "Systematic accounts for *Trilepida*" in a further section below).

A statolithic mass in the *cavum vestibuli* is always present in *Trilepida* spp. (Pinto et al., 2015; Salazar-Valenzuela et al., 2015; present study). In Serpentes, a statolithic mass is associated with the lumen of a saccular statocony membrane, which is composed of a delicate gelatinous matrix of densely compacted statoconia (Baird, 1970). Although the function of the saccular matrix is not yet well known, it may be associated with equilibrium or even with a function of hearing, receiving anterior and posterior branches of the vestibulocochlear nerve (Baird, 1970). Both functionalities associated with hearing (through ground vibrations) and equilibrium, which allow for better positioning accuracy in the underground, should be considered plausible for threadsnakes and other taxa that exhibit these structures.

4.2 | Suspensorium and lower jaw

As in other Leptotyphlopidae (Kley, 2006; List, 1966; McDowell and Bogert, 1954; Pinto et al., 2015; Rieppel et al., 2009), the mandible is subterminal, short, and suspended from the skull by the quadrates, which are associated with the skull by a series of cartilages, ligaments, and muscles (Kley, 2006; Martins, Passos, et al., 2019). The absence of a bone connection to the skull seems to suggest translational movements of the quadrate (McDowell, 2008), providing a more efficient underground feeding apparatus. The members of the genus *Trilepida* exhibit reduced inter- and intraspecific variability of the lower jaw, except for the presence/absence of foramina, number of teeth, and shape of coronoid. The intraspecific variability in relation to the number of teeth has already been reported in the literature (List, 1966; Pinto et al., 2015), although the condition in which the dentary bears five or six teeth seems to be a more common pattern not only for *Trilepida* spp., but also for other leptotyphlopids (Koch et al., 2019; List, 1966; Pinto et al., 2015; Rieppel et al., 2009; Salazar-Valenzuela et al., 2015; present study).

The morphological complexity of the coronoid is typical for members of Leptotyphlopidae (List, 1966; Rieppel et al., 2009), with the element exhibiting three processes: the dorsal, the surangular, and the prearticular process (Kley, 2006; List, 1966; Pinto et al., 2015; Rieppel et al., 2009). This complexity and variability might reflect intrinsic functional demands generated by the insertion area of the *Musculus adductor externus medialis* complex, pars "a", "b," and "c" (sensu Martins, Passos, et al., 2019). The dorsal process is essentially spoon-shaped in all *Trilepida* species, even though all herein analyzed specimens of *T. macrolepis* exhibit three processes. Additional samples in future studies might help to elucidate if this character state is autapomorphic for the species, providing distinct areas for the attachment of the *M. adductor externus medialis* complex, pars "a", "b," and "c" (sensu Martins, Passos, et al., 2019).

Several authors report the presence of a cartilaginous region associated with the posterior portion of the proximal quadrate head (Kley, 2006; List, 1966; Pinto et al., 2015). A possible cartilage with proximal calcification led Kley (2006)—based on the premises of Maisano (2002)—to propose that this cartilage might represent epiphyses. Pinto et al. (2015) corroborate this idea by reporting calcified proximal epiphyses in *T. salgueiroi*. According to Kley (2006) (and later confirmed by Pinto et al., 2015), if these cartilages represent in fact epiphyses, then this characteristic would constitute an additional heterochronic (i.e., paedomorphic) feature for the Scolecophidia. The results obtained in the present study

corroborate this assumption. In several species examined, a cartilage located distal to the proximal region of the quadrate is present and well calcified, even being visible in several tomographed specimens. If this cartilage associated with the quadrate actually represents an epiphysis, the retention of the paedomorphic character would be limited to the New World taxa (*Rena* and *Trilepida*; present study), and to Rhinoleptini (*Rhinoleptus* + *Tricheilostoma*; List, 1966; Martins, 2016). According to the illustrations by List (1966), *Leptotyphlops* also exhibits a ventroposterior extension of the quadrate, suggesting that this genus does not retain this paedomorphic condition. However, additional studies including a representative sample of species belonging to Leptotyphlopinae are needed.

4.3 | Postcranial osteology

Study of postcranial osteology, especially comprising the vertebrae of Scolecophidia, is scarce in the literature. After the work of List (1966), studies providing detailed information on the axial osteology of Leptotyphlopidae include, as far as we are aware, only those of Pinto et al. (2015), Salazar-Valenzuela et al. (2015), Koch et al. (2019), and Martins, Koch, et al. (2019). Additional descriptive studies on the leptotyphlopid vertebrae morphology come from few paleontological features of fossil snakes (Holman, 2000; Ikeda, 2007; Mead, 2013; Van Devender & Mead, 1978; Van Devender & Worthington, 1977). On the other hand, literature data combined with the data generated herein suggest that the morphology of trunk, cloacal, and caudal vertebrae in Scolecophidia is highly conserved (Holman, 2000; Ikeda, 2007; List, 1966; Mead, 2013).

The cervical vertebrae (atlas and axis) display relative variation on the inter- and intraspecific levels. Most variation mainly concerned the shape and condition of the intercentra II and III, and many of the inter- and intraspecific variabilities have already been reported or illustrated in the literature for members of Leptotyphlopidae (List, 1966; Pinto et al., 2015). Although interspecific variability in axis morphology is relatively well documented in other Squamata (Cernansky et al., 2014; Conrad, 2006), the available studies for snakes still do not fulfill this scenario. The absence of a well-developed neural spine in the trunk vertebrae of all "Scolecophidia" has already been attributed in the literature to fossorial habits (Groombridge, 1979; Rieppel, 1988; Underwood, 1967), also occurring along the Alethinophidia lineages with fossorial or semi-fossorial lifestyles (Rieppel, 1988).

In Squamata, the cloacal region is characterized by a series of vertebrae bearing bifurcated ribs that are laterally fused to the *centrum* and what are called lymphapophyses (Renous et al., 1991; Romer, 1956). These vertebrae accommodate the "lymphatic hearts," which extend over a variable number of cloacal vertebrae and might reach the sacral region (Gasc, 1967). There is a presence of musculature between the arms of the lymphapophyses, providing a cloistered and protected region for these lymphatic hearts. However, the relation of the presence of these "lymphatic hearts" with their participation in locomotion of elongated reptiles is not yet clear. In Serpentes as a rule, "heart lymphatic cells" are well-developed, extending up to seven cloacal vertebrae posteriorly, and may even reach posterior thoracolumbar vertebrae (= sacral vertebrae), since a dissociation of the rudimentary pelvic elements with the spine does not provide a barrier to its anterior stretching (Renous et al., 1991). The range of variation in the number of cloacal vertebrae in *Trilepida* spp. is in accordance with the snake pattern (up to seven cloacal vertebrae), varying from three to five, and bearing a short cartilage in the distal region of each arm of the lymphapophysis (Fabrezi et al., 1985; List, 1966; Pinto et al., 2015; present study). The caudal vertebrae show no conspicuous morphological variation within the genus *Trilepida*.

All species examined herein exhibit the W-shaped pattern for the costal cartilages of the trunk vertebrae, as observed in Alethinophidia (Hardaway & Williams, 1976). Pinto et al. (2015) have provided detailed data on the anteroposterior variation of the costal cartilages shape in a perspective of variation of the anchoring for the *Musculus costocutaneous inferior*. Herein, we have also noticed an anterior–posterior variation in terms of cartilage shape, reinforcing the need of myological studies that correlate possible muscular variations in cartilage shape.

4.4 | Rudimentary pelvic and hindlimb elements

The origin of the snake-like *bauplan* from a four-legged lizard ancestor has triggered the evolution of several features such as body elongation and limb loss. Even though the regulatory mechanisms that involve the forelimb and hindlimb loss are still poorly understood (Leal & Cohn, 2017), the presence of vestiges in most basal snakes indicates that these elements were reduced before undergoing a complete elimination during the snake evolution (Apesteguia & Zaher, 2006; Leal & Cohn, 2017). This scenario suggests that the mechanisms of limb development were not completely lost in snakes (Leal & Cohn, 2016), even though the selection to maintain preexisting functions in the

external genitalia was possibly the force that acted to preserve many of these limb enhancers (Infante, Rasys, & Menke, 2018).

The diversity of pelvic and hindlimb rudiments in Squamata has long been reported and studied (Palci et al., 2019; Renous et al., 1991), with the homology of these components being historically a matter of debate (Palci et al., 2019). A recent study (Palci et al., 2019) has provided relevant data on the evolutionary processes of reduction in the pelvis and hindlimbs of snakes, providing consistent data on the homology of these elements, which have been gained and lost several times across the evolutionary history of snakes.

The degree of degeneration of pelvic and hindlimb elements is highly variable in snakes, with a yet obscure and unpredictable variability among taxa, as also found herein for *Trilepida* spp. (Essex, 1927; List, 1966; Palci et al., 2019; Renous et al., 1991; Roscito & Rodrigues, 2013; present study). The high variability in their shape and composition most likely points to a feasible current functional interaction of these elements rather than a merely vestigial retention without any functional operation (Palci et al., 2019).

Members of the genus *Trilepida*—as other Leptotyphlopidae—exhibit a low degree of degeneration of pelvic and hindlimb elements among snakes in general (Essex, 1927; List, 1966; Palci et al., 2019), with four ossified (and rarely cartilaginous) distinctive elements (ilium, ischium, pubis and femur), with the femur being surrounded by a rigid claw-shaped cover also known as the femoral spur (Palci et al., 2019). The inconspicuous degeneration most likely indicates that leptotyphlopids retain the most plesiomorphic condition of pelvic and hindlimb elements among snakes (Palci et al., 2019; present study), which are shared with other taxa such as *Cylindrophis* and a few boids (Palci et al., 2019). According to Palci et al. (2019), the snake common ancestor lacked pelvic or hindlimb rudiments, with these features convergently re-evolving independently several times within the snake radiation. One likely scenario includes multiple gains of elements of the pelvis and hindlimb, occurring at least twice in snakes: once in Alethinophidia and the other time in Leptotyphlopidae (Palci et al., 2019). Therefore, the retention of ossified or even cartilaginous elements presumably indicates a functional usage in Leptotyphlopidae that demands further investigation.

4.5 | Cartilaginous elements

Data on the cartilaginous elements associated with the skull or cephalic region (i.e., nasal cartilages, *trabeculae cranii*, hypobranchial apparatus, larynx, glottal tube and trachea) are as a rule relatively scarce compared to the descriptive works on cranial and postcranial osteology in snakes. Although the description of these elements is usually hampered by the traditional use of invasive methods (i.e., clearing and staining), many osteological works that applied cleared and stained methods to describe the osteology of scolecophidians do not provide descriptive data for these cartilaginous structures, and thus are limited to osteology exclusively.

The nasal cartilage represents one of the least studied cartilaginous structures in snakes (Di Pietro et al., 2014; Pinto et al., 2015), with most studies being focused on Alethinophidia (De Beer, 1937; Kamal & Hammouda, 1965a,b,c; Pringle, 1954; Scrocchi et al., 1998). Bellairs and Kamal (1981) have compiled descriptive works on the nasal cartilage, synthesizing general morphological patterns for Caenophidia but without information for scolecophidians. In the present study, we provide a characterization of the nasal, hypochoanal, and ectochoanal cartilages for *Trilepida* species, which are consistently similar to that previously reported by Pinto et al. (2015), indicating that these structures are very conserved at least in the genus (present study). Therefore, future studies with wider sample size might unveil whether these characters are useful for the systematics of threadsnakes, as it has previously been hypothesized for other Alethinophidia (Di Pietro et al., 2014). Still, the lateral expansion of both *planum orbitale* and parietotectal cartilages found herein seems to be associated with the well-developed nasal complex elements, and thus this condition might be present in other scolecophidians (present study).

The ossification of the hypochoanal and ectochoanal cartilages has led to several discussions regarding their homology, putative association to an ectopterygoid, or even heterotopic ossification in Leptotyphlopidae (List, 1966; Pinto et al., 2015). Based on cleared and stained specimens and tomography images, we suggest the standardization of terminology of these elements as hypochoanal and ectochoanal cartilages for leptotyphlopids. Even though the ectochoanal and hypochoanal cartilages are both always present in Serpentes, the posterior fusion of these elements into a wide plate is not present in many snake taxa (Bellairs & Kamal, 1981). Herein, we hypothesize that the fusion and ossification might be related to resistance demands on the mouth roof during feeding (that might include much rigid soil debris), as it occurs in a few "lizard" taxa such as *Xantusia vigilis* (Bellairs & Kamal, 1981). As in all snakes (McDowell, 1972), the ectochoanal cartilage is dissociated from the maxilla, which is evolutionarily associated with supposedly higher maxillae mobility. However, the immobile maxillae of

leptotyphlopids suggest that the loss of maxillary mobility is secondarily evolved from an ancestor with maxillary mobility.

The hyoid is a derivative of the hypobranchial apparatus and performs the primary function of posterior support of the musculature associated with the tongue (*hyoglossi*). It further supports muscles associated with the mandible, cutaneous region, nuchal, and anterior ribs in snakes (Langebartel, 1968). The hyoid shape in Serpentes is variable ("Y", "V", "M," or parallel), located in the anteroventral region of the skull and under the "nuchal" region. Compared to other snakes, leptotyphlopids and typhlopids exhibit posterior-located hyoids (List, 1966; Langebartel, 1968; Pinto et al., 2015; present study), which represent a unique condition among gnathostomatans (Underwood, 1967). Although this condition has been hypothesized as a derived character in these groups (Kluge, 1976), the issue on the evolution of this condition remains unresolved (Groombridge, 1979). However, if a posterior displacement of the hyoid is associated with anchorage of the tongue and, consequently, directly related to food intake, this condition most likely evolved in parallel, considering both taxa exhibit extremely divergent feeding mechanisms (Iordansky, 1997; Kley, 2001, Kley, 2006; Mizuno & Kojima, 2015).

The reduced variability found in the hyoid among *Trilepida* spp. was basically associated to the relative size between the lingual process and the cornua. Even though the relative morphological stability of the hyoid in leptotyphlopids has been referred as having no phylogenetic value (Langebartel, 1968), when considering the possible morphofunctional aspects related to hyoid size, one must concede that they might generate complementary utility for muscle function, as follows. The lingual process and the cornua provide support for the origin of musculature in the ventral region of the head and musculature associated with the tongue. Each element can give exclusive support to muscle complexes, such as *Musculus genioglossus* and the medial bundle of *Musculus ceratomandibularis* (see Martins, Passos, et al., 2019). Differences in the size of these elements might lead to different levels of muscle stability, so that the total absence of one of these elements (as occurs in Typhlopidae) most likely results in a rearrangement or overlap of the insertion points of these muscles.

The larynx and the glottal tube are morphologically similar among *Trilepida* species. As described for *T. salgueiroi* (Pinto et al., 2015), the larynx has well-developed arytenoid cartilages being approximately subtriangular or semicircular in shape, and lies dorsally to the anterior limit of the glottal tube. The cricoid cartilage is located ventroanteriorly to the arytenoid cartilages and, despite presenting slightly variable shape, it projects anteriorly to the arytenoid cartilages. Both qualitative characters of the larynx and quantitative data on the glottal tube show a high degree of intraspecific variability, as previously pointed out by Pinto et al. (2015), thus leading to a reduced phylogenetic value of these characters for leptotyphlopids, and contrasting with its systematic use in Alethinophidia (Di Pietro et al., 2014).

In all species examined, tracheal rings are type I and C-shaped. We observed three patterns regarding the width of the rings/interspace: the first, which is common in basal groups of snakes and/or reptiles of fossorial habits, retains wide rings with short interspaces, with the cartilages being at least three times larger than the interspaces. This condition was observed in *T. fuliginosa* and *T. jani*. A second pattern of moderate tracheal rings was observed in *T. brasiliensis*, *T. dimidiata*, *T. joshuai*, and *T. koppesi*, while thin rings were found exclusively in *T. macrolepis*. Considering there is a clear anterior–posterior modification between the interspaces, the variability observed herein might reflect the clear alteration of these measures along the trachea of individuals. Considering the limited evidence available to date, we are still not able to assume whether these variations also occur intraspecifically, a topic which must be addressed in future studies.

4.6 | Systematic implications for the genus *Trilepida*

The genus *Trilepida* was recognized and diagnosed considering the phylogenetic hypothesis of Adalsteinsson et al. (2009) that only included three specimens of *T. macrolepis* (the type species of the genus). Several scalation characters have been proposed to diagnose the genus in comparison to its congeners, although they were subsequently criticized by a few authors (Pinto, 2010; but see first paragraph of this subsection). Since then, the proposed taxon has had no compelling diagnostic features for its recognition, even though Passos et al. (2006) and Pinto et al. (2010) have suggested that some hemipenial characters might be synapomorphic for the genus. Although characters have not yet been phylogenetically tested, our representative sample of *Trilepida* species combined with published data allows us to propose an osteological diagnosis based on a combination of characters that is unique for the genus. These diagnostic features are mostly associated to the conditions of the parietals, nasals, supraoccipitals, and basioccipital, and will be discussed in the following paragraphs in comparison to other Epictinae.

4.6.1 | The parietal condition

In all species of *Trilepida*, the parietals are represented by a single and fused element, as with other Epictinae (Koch et al., 2019; List, 1966; Pinto et al., 2015; Rieppel et al., 2009; Salazar-Valenzuela et al., 2015). It can be distinguished from a few *Rena* by the absence of a dorsal fontanelle (List, 1966; Martins, 2016), and from *Tetracheilostoma* by having the parietal as an element that is not fused to the supraoccipital (see Martins et al., This volume).

4.6.2 | The basioccipital condition

The basioccipital is, in almost all *Trilepida* spp., included in the ventral medial limit of the foramen magnum, precluding the otooccipitals to meet ventrally. However, *T. nicefori* seems to exhibit a distinct condition in relation to other congeners in exhibiting the otooccipitals in ventral contact to exclude the basioccipital from the formation of the foramen magnum. This condition has been previously reported and/or illustrated for *Epictia*, *Habrophallos*, and *Rena* (Fabrezi et al., 1985; Koch et al., 2019; List, 1966; Martins, Koch, et al., 2019; Rieppel et al., 2009) and, except for *T. nicefori*, does not seem to vary intragenerically among Epictinae (Martins, 2016).

4.6.3 | The nasals condition

In Leptotyphlopidae, the nasals might be paired or fused into a single unit, although the first condition seems to be the most common among lineages of this family (Broadley & Wallach, 2007; Brock, 1932; Fabrezi et al., 1985; List, 1966; Martins, 2016). Regarding Epictinae, exclusively members of the genera *Epictia*, *Habrophallos*, and *Rena* (Koch et al., 2019; List, 1966; Martins, 2016; Martins, Koch, et al., 2019; Rieppel et al., 2009) exhibit fused nasals, even though they might be paired in a few enigmatic taxa of the latter (Martins, 2016). All *Trilepida* spp. evaluated herein exhibited invariably paired nasals that do not expand laterally, being medially delimitated by a conspicuous suture.

4.6.4 | The supraoccipital condition

The presence of fused supraoccipitals that are distinct from the parietals and otooccipitals seem to be uncommon among Epictinae (see Koch et al., 2019; List, 1966; Martins, Koch, et al., 2019). The fused condition occurs in *Habrophallos* (Martins, Koch, et al., 2019), while in *Tetracheilostoma* it appears to be fused to the parietal (Martins et al., This volume). A few variations in the condition of supraoccipitals (Koch et al., This volume; List, 1966; Martins et al., This volume; Rieppel et al., 2009) indicate that these elements must be considered for systematic purposes, since these elements seem to be intergenerically invariable (Martins, 2016; present study).

Considering that the conditions found in the parietal, nasals, supraoccipitals, and basioccipital do not vary intragenerically among Epictinae (Martins, 2016), we believe these characters are systematically relevant for diagnosing this genus. Therefore, we propose that the following combination of osteological characters unequivocally distinguishes the genus *Trilepida* from other Epictinae: (a) presence of a single parietal which is not fused to any element (vs. fused to supraoccipital in *Tetracheilostoma*; see Martins et al., This volume); (b) parietal fontanelle absent (vs. present in a few *Rena*; see Martins, 2016); (c) paired nasals (vs. fused in a few *Rena* and a few *Epictia*; List, 1966; Rieppel et al., 2009); (d) supraoccipitals fused as a single unit that is distinct from the parietal and otooccipitals (vs. paired in *Epictia*, *Rena*; fused to parietal in *Tetracheilostoma*); (e) the basioccipital participating in the formation of the foramen magnum (except for *T. nicefori*; vs. not participating in *Epictia* and *Habrophallos*); and (f) the prootics being distinct from the otooccipitals (vs. indistinct in *Mitophis* and *Tetracheilostoma*; Martins et al., This volume). This combination of characters does not occur in any other Epictinae (Koch et al., This volume; List, 1966; Martins, 2016; Martins et al., This volume; Rieppel et al., 2009), and must be considered in future studies as they will certainly be valuable for resolving several phylogenetic positioning issues (Koch et al., This volume), as it has already been applied for the description of new taxa (Koch et al., 2019; Martins, Koch, et al., 2019; Salazar-Valenzuela et al., 2015). If the ancestral condition of the basioccipital in leptotyphlopids indeed encompasses the exclusion of the basioccipital in the formation of the foramen magnum, then *T. nicefori* might exhibit a clear reversal of this condition in comparison to all other species of *Trilepida* known, being an autapomorphy of the species. Additionally, this species seems to exhibit a few further exclusive osteological characteristics that distinguish it from other *Trilepida* spp., such as the foramen for the *apicalis nasi* being posterior and formed by the frontals, the absence of an intercentrum I, reduced trigeminal nerve foramen and the prearticular lamina of coronoid being extremely reduced (present study). The external morphology of the species (Pinto, 2010; Pinto &

Fernandes, 2012) is also distinct from other species of *Trilepida*, mostly by having a reduced number of dorsal and ventral scales (167–168) and by the presence of three infralabials (vs. four in all other *Trilepida*; Pinto, 2010; Pinto & Fernandes, 2012). Additional data on trans-Andean species not examined herein (i.e., *T. anthracina*, *T. brevissima*, and *T. dugandi*) might elucidate the nature of this variation and must be considered in future studies.

Finally, during the osteological examination of the holotype of *T. guayaquilensis*, we have observed that the skull features were not consistent with the skull data proposed herein as diagnostic for the genus *Trilepida*. This species is currently known exclusively from its holotype and Pinto et al. (2010) has previously questioned its generic allocation. Given the congruent combination of external morphology and osteological data, the generic reassessment of *T. guayaquilensis* was addressed elsewhere (Koch et al., 2021). Thus, one must acknowledge that the high representativeness of species ($n = 12$) and specimens ($n = 47$) of the genus analyzed herein allows us to provide a comprehensive comparison and discussion with respect to 11 (by excluding *T. guayaquilensis*) out of the 14 species currently recognized as pertaining to the genus *Trilepida*. Lastly, we encourage future taxonomic studies on threadsnakes to combine detailed anatomical with external morphological data to provide accurate systematic evidence and robust diagnostic features for considered taxa.

ACKNOWLEDGMENTS

We are thankful to the following persons for allowing us to examine specimens under their care: F.L. Franco, F. Grazziotin and G. Puorto (IBSP), H. Zaher (MZUSP), A.L.C. Prudente (MPEG), F.F. Curcio (UFMT), G. Colli and M. Zatz (CHUNB), M. Pires (LZV/UFOP), R. Feio (MZUFV), C. Raxworthy (AMNH), A. Resetar (FMNH), K. de Queiroz, R. Wilson, R. McDiarmid and A. Wynn (USNM), C. Phillips (UIMNH), J.L. Watters (OMNH), R. Brown (KU), B. Hollingsworth (SDMNH), N. Camacho (LACM), J. Rosado (MCZ), O. Torres-Carvajal (QCAZ), S. Kretzschmar (FML), P. Campbell (BMNH), F. Tillack and M. Rödel (ZMB), S. Schweiger and G. Gassner (NHMW), N. Vidal (MNHN), O. Pauwels (RBINS). The holotype of *Trilepida brasiliensis* was imaged by J. Smith using the digitization facility of the RBINS in the framework of the DIGIT04 project funded by BELSPO and J. Brecko provided us with the CT scan data. To P. Prado and M. Folly for data on vertebrae counts. Angele Martins is grateful to K. de Queiroz, D. Johnson, A. Nonaka, R. McDiarmid, R. Wilson, and all USNM staff for the support during the conduction of the project in the United States.

AUTHOR CONTRIBUTIONS

Claudia Koch: Investigation (equal); methodology (equal); software (equal); validation (equal); visualization (equal); writing – original draft (equal); writing – review and editing (equal). **Mitali Joshi:** Methodology (equal); software (equal); writing – review and editing (equal). **Roberta Pinto:** Conceptualization (equal); project administration (equal); supervision (equal); validation (equal); writing – review and editing (equal). **Paulo Passos:** Conceptualization (equal); data curation (equal); funding acquisition (equal); methodology (equal); project administration (equal); resources (equal); supervision (equal); writing – review and editing (equal).

ORCID

Angele Martins https://orcid.org/0000-0002-0193-4011
Claudia Koch https://orcid.org/0000-0002-7115-2816

REFERENCES

Adalsteinsson, S. A., Branch, W. R., Trape, S., Vitt, L. J., & Hedges, S. B. (2009). Molecular phylogeny, classification, and biogeography of snakes of the family Leptotyphlopidae (Reptilia, Squamata). *Zootaxa*, *2244*, 1–50.

Apesteguia, S., & Zaher, H. (2006). A cretaceous terrestrial snake with robust hindlimbs and a sacrum. *Nature*, *440*, 1037–1040.

Baird, I. L. (1970). The anatomy of the reptilian ear. In C. Gans & T. S. Parsons (Eds.), *Biology of the Reptilia, Vol 2. (Morphology B)* (pp. 193–275). New York: Academic Press.

Bellairs, A. A., & Kamal, A. M. (1981). The chondrocranium and the development of the skull in recent reptiles. In C. Gans & T. S. Parsons (Eds.), *Biology of Reptilia, Vol 11* (pp. 1–263). London, UK: Academic Press.

Broadley, D. G., & Broadley, S. (1999). A review of the African worm snakes from south of latitude 12°S (Serpentes: Leptotyphlopidae). *Syntarsus*, *5*, 1–36.

Broadley, D. G., & Wallach, V. (2007). A revision of the genus *Leptotyphlops* in northeastern Africa and southwestern Arabia (Serpentes: Leptotyphlopidae). *Zootaxa*, *1408*, 1–78.

Brock, G. T. (1932). The skull of *Leptotyphlops* (*Glauconia nigricans*). *Anatomischer Anzeiger*, *73*, 199–204.

Brongersma, L. D. (1958). Upon some features of the respiratory systems in the Typhlopidae and some other snakes. *Archives Néerlandaises de Zoologie*, *13*, 120–127.

Čerňanský, A., Boistel, R., Fernandez, V., Tafforeau, P., Nicolas, L. N., & Herrel, A. (2014). The atlas-axis complex in chamaeleonids (squamata: chamaeleonidae), with description of a new anatomical structure of the skull. *The Anatomical Record*, *297*(3), 369–396. http://doi.org/10.1002/ar.22859

Conrad, J. L. (2006). Postcranial skeleton of Shinisaurus crocodilurus (Squamata: Anguimorpha). *Journal of Morphology*, *267*(7), 759–775. http://doi.org/10.1002/jmor.10291

Cundall, D., & Greene, H. W. (2000). Feeding in snakes. In K. Schwenk (Ed.), *Feeding: Form, function and evolution in tetrapod vertebrates* (pp. 293–333). San Diego, CA: Academic Press.

Cundall, D., & Irish, F. (2008). The snake skull. In C. Gans, A. S. Gaunt, & K. Adler (Eds.), *Biology of the Reptilia, Vol.*

20, Morphology H (pp. 349–692). New York: Society for the Study of Amphibians and Reptiles.

Cundall, D., & Rossman, D. A. (1993). Cephalic anatomy of the rare Indonesian snake *Anomochilus weberi*. *Zoological Journal of the Linnean Society*, *109*, 235–273.

De Beer, G. (1937). *The development of the vertebrate skull*. 1, 1, (1–622). Chicago: University of Chicago Press.

Deolindo, V., Koch, C., Joshi, M., & Martins, A. (2021). To move or not to move? Skull and lower jaw morphology of the blindsnake Afrotyphlops punctatus (Leach, 1819) (Serpentes, Typhlopoidea, Typhlopidae) with comments on its previously advocated cranial kinesis. *The Anatomical Record*, http://doi.org/10.1002/ar.24598

Di Pietro, D. O., Alcalde, L., & Williams, J. D. (2014). Nasal cartilages, hyobranchial apparatus, larynx, and glottal tubes in four species of Hydropsini (Serpentes: Dipsadidae: Xenodontinae). *Vertebrate Zoology*, *64*(1), 103–111.

Duerden, J. E., & Essex, R. (1923). The pelvic girdle in the snake *Glauconia*. *South African Journal of Science*, *20*, 354–356.

Duméril, A. M. C. (1853). *Prodrome de la classification des Reptiles phidiens*. Paris, France: Librarie Encyclopédique de Roret.

Dunn, E. R. (1941). Notes on the snake genus Anomalepis. *Museum of Comparative Zoology*, *87*, 511–526.

Dunn, E. R., & Tihen, A. (1944). The skeletal anatomy of Liotyphlops albirostris. *Journal of Morphology*, *74*, 287–295.

Essex, R. (1927). Studies in reptilian degeneration. *Proceedings of the Zoological Society of London*, *4*, 879–945.

Fabrezi, M., Marcus, A., & Scrocchi, G. (1985). Contribución al conocimiento de los Leptotyphlopidae de Argentina. I. *Leptotyphlops weyrauchi* y *Leptotyphlops albipuncta*. *Cuadernos de Herpetologica*, *1*, 1–20.

FitzSimons, V. F. M. (1962). *Snakes of Southern Africa*. Cape Town, South Africa: Purnel and Sons.

Gans, C. (1961). The feeding mechanism of snakes and its possible evolution. *American Zoologist*, *1*, 217–227.

Gasc, J. (1967). Retentissement de l'adaptation a la locomotion apode sur le squelette des squamates. In: *Coll. Evolution des vertebres*, (Vol. 163, pp. 360–380). Paris: Cooloq Int Cent Nat Rech.

Gauthier, J. A., Kearney, M., Maisano, J. A., Rieppel, O., & Behlke, A. D. (2012). Assembling the Squamate tree of life: Perspectives from the phenotype and the fossil record. *Bulletin of the Peabody Museum of Natural History*, *53*, 3–308.

George, H. (1959). Bemerkungen über die Anatomie des Kopfes und des Schadels der Leptotyphlopidae (Ophidia) speciell von L. macrorhynchus Jan. *Vierteljahrsschrift der Naturforschenden Gesellschaft in Zürich*, *104*, 90–104.

George, H. (1964). Anatomical observations on the head of Liotyphlops albirostris (Typhlopidae, Ophidia). *Acta Zoologica*, *45*, 1–62.

George, H. (1968). Anatomical observations on the head of Anomalepis aspinosus (Typhlopidae, Ophidia). *Acta Zoologica*, *49*, 62–139.

Greene, H. W. (1997). *Snakes: The evolution of mystery in nature*. Berkeley: University of California Press.

Groombridge, B. (1979). A previously unreported throat muscle in Scolecophidia (Reptilia: SErpentes), with comments on other scolecophidian throat muscles, *13*, 447–475.

Hardaway, T. E., & Williams, K. L. (1976). Costal cartilages in snakes and their phylogenetic significance. *Herpetologica*, *32*, 378–387.

Holman, J. A. (2000). *Fossil snakes of North America: Origin, evolution, distribution, paleoecology*. Indiana: Indiana University Press.

Infante, C., Rasys, A., & Menke, D. (2018). Appendages and gene regulatory networks: Lessons from the limbless. *Genesis*, *56*, e23078.

Ikeda, T. (2007). A comparative morphological study of the vertebrae of snakes occurring in Japan and adjacent regions. *Current Herpetology*, *26*(1), 13–34.

Jan, G., & Sordelli, F. (1861). *Iconographie Générale des Ophidiens*. Paris, France: JB Ballière et Fils.

Kamal, A., & Hammouda, H. (1965a). The development of the skull of Psammophis sibilans. I. The development of the chondrocranium. *Journal of Morphology*, *116*, 197–246.

Kamal, A., & Hammouda, H. (1965b). The development of the skull of Psammophis sibilans. II. The fully formed chondrocranium. *Journal of Morphology*, *116*, 247–295.

Kamal, A., & Hammouda, H. (1965c). Observations on the chondrocranium of the snake, Cerastes vipera. *Gegenbaurs Morphologisches Jahrbuch*, *107*, 58–97.

Kley, N. J. (2006). Morphology of the lower jaw and suspensorium in the Texas blindsnake, *Leptotyphlops dulcis* (Scolecophidia: Leptotyphlopidae). *Journal of Morphology*, *267*, 494–515.

Kley, N. J., & Brainerd, E. L. (1999). Feeding by mandibular raking in a snake. *Nature*, *402*, 369–370.

Kluge, A. (1976). Phylogenetic relationships in the lizard family Pygopodidae: an evaluation of theory, methods and data. *Miscellaneous publications (University of Michigan. Museum of Zoology)*, *152*, 1–72.

Koch, C., Martins, A. R., & Schweiger, S. (2019). A century of waiting: Description of a new *Epictia* Gray, 1845 (Serpentes: Leptotyphlopidae) based on specimens housed for more than 100 in the collection of the Natural History Museum Vienna (NMW). *PeerJ*, *7*, e7411. https://doi.org/10.7717/peerj.7411

Koch, C., Martins, A., Joshi, M., Pinto, R. R., & Passos, P. (2021). Osteology of the enigmatic threadsnake species Epictia unicolor and Trilepida guayaquilensis (Serpentes: Leptotyphlopidae) with generic insights. *The Anatomical Record*. http://doi.org/10.1002/ar.24676

Langebartel, D. A. (1968). The hyoid and its associated muscles in snakes. *Illinois Biological Monographs*, *38*, 1–156.

Lapage, E. O. (1928). The septomaxillary of the Amphibia Anura and of the Reptilia. *Journal of Morphology and Physiology*, *46*, 399–430.

Leal, F., & Cohn, M. (2016). Loss and re-emergence of legs in snakes by modular evolution of sonic hedgehog and hoxd enhancers. *Current Biology*, *26*, 2966–2973.

Leal, F., & Cohn, M. (2017). Developmental, genetic, and genomic insights into the evolutionary loss of limbs in snakes. *Genesis*, *56*, 1–12. https://doi.org/10.1002/dvg.23077

Lee, M. S., & Scanlon, J. D. (2002). Snake phylogeny based on osteology, soft anatomy and ecology. *Biological Reviews of the Cambridge Philosophical Society*, *77*, 333–401.

Lee, M. S., Hugall, A. F., Lawson, R., & Scanlon, J. D. (2007). Phylogeny of snakes (Serpentes): Combining morphological and molecular data in likelihood, Bayesian and parsimony analyses. *Systematics and Biodiversity*, *5*, 371–389.

Lira, I., & Martins, A. (2021). Digging into blindsnakes' morphology: Description of the skull, lower jaw, and cervical vertebrae of two Amerotyphlops (Hedges et al., 2014) (Serpentes,

Typhlopidae) with comments on the typhlopoidean skull morphological diversity. *The Anatomical Record*. http://doi.org/10.1002/ar.24591

List, J. C. (1955). External limb vestiges in *Leptotyphlops*. *Herpetologica*, *11*, 15–16.

List, J. C. (1966). Comparative osteology of the snake families Typhlopidae and Leptotyphlopidae. *Illinois Biological Monographs*, *36*, 1–112.

Maisano, J. A. (2002). Terminal fusions of skeletal elements as indicators of maturity in squamates. *Journal of Vertebrate Paleontology*, *22*(2), 268–275. http://doi.org/10.1671/0272-4634(2002)022[0268:tfosea]2.0.co;2.

Martins, A. R. (2016). *Morfologia Interna Comparada de Representantes da Subfamília Epictinae (Serpentes, Scolecophidia, Leptotyphlopidae)*. (Unpublished thesis). Rio de Janeiro, Brazil.

Martins, A. R., Passos, P., & Pinto, R. (2018). Unveiling diversity under the skin: Comparative morphology study of the cephalic glands in threadsnakes (Serpentes: Leptotyphlopidae: Epictinae). *Zoomorphology*, *137*, 433–443.

Martins, A. R., Koch, C., Pinto, R., Folly, M., Fouquet, A., & Passos, P. (2019). From the inside out: Discovery of a new genus of threadsnakes based on anatomical and molecular data, with discussion of the leptotyphlopid hemipenial morphology. *Journal of Zoological Systematics and Evolutionary Research*, *57*, 840–863.

Martins, A. R., Passos, P., & Pinto, R. (2019). Moving beyond the surface: Comparative head and neck myology of threadsnakes (Epictinae, Leptotyphlopidae, Serpentes), with comments on the 'scolecophidian' muscular system. *PLoS One*, *14*, e0219661.

Martins, A. R., Koch, C., Pinto, R. R., & Passos, P. (This volume). Evolutionary treasures hidden on West Indies: comparative osteology and visceral morphology reveals intricate miniaturization on the insular genera *Mitophis* Adalsteinsson, Hedges & Branch, 2009 and Tetracheilostoma Jan, 1861 (Leptotyphlopidae: Epictinae: Tetracheilostomina).

McDowell, S. B. (1972). The evolution of the tongue of snakes and its bearing on snake origins. In T. Dobzhansky, M. Hecht, & W. Steere (Eds.), *Evololutionary biology* (Vol. 6, pp. 191–273). New York: Springer.

McDowell, S. B. (1974). A catalogue of the snakes of New Guinea and the Solomons, with special reference to those in the Bernice P. Bichop Museum. I. Scolecophidia. *Journal of Herpetology*, *8*, 1–57.

McDowell, S. (2008). The skull of Serpentes. *Biology of Reptilia*. 21, 1, (467–620). Ithaca: Society for the Study of Amphibians and Reptiles.

McDowell, S., & Bogert, C. (1954). The systematic position of Lanthanotus and the affinities of the anguinomorphan lizards. *Bulletin of the American Museum of Natural History*, *105*, 1–142.

Mead, J. (2013). Scolecophidia (Serpentes) of the late Oligocene and early Miocene, North America, and a fossil history overview. *Geobios*, *46*, 225–231.

Miller, M. R. (1968). The cochlear duct of snakes. *Proceedings of the California Academy of Sciences, 4th series*, *35*, 425–476.

Miralles, A., Marin, J., Markus, D., Herrel, A., Hedges, S. B., & Vidal, N. (2018). Molecular evidence for the parapyly of Scolecophidia and its evolutionary implications. *Journal of Evolutionary Biology*, *31*, 1782–1793.

Mizuno, T., & Kojima, Y. (2015). A blindsnake that decapitates its termite prey. *Journal of Zoology*, *297*(3), 220–224. http://doi.org/10.1111/jzo.12268

Palci, A., & Caldwell, M. (2013). Primary homologies of the circumorbital bones of snakes. *Journal of Morphology*, *27*, 973–986.

Palci, A., Hutchinon, M., Caldwell, M., Smith, K., & Lee, M. (2019). The homologies and evolutionary reduction of the pelvis and hindlimbs in snakes, with the first report of ossified pelvic vestiges in an anomalepidid (*Liotyphlops beui*). *Zoological Journal of the Linnean Society*, *188*, 1–23.

Parker, H. W., & Grandison, A. G. (1977). *Snakes: A natural history*. London, UK: British Museum (Natural Hisotry) and Cornell University Press.

Passos, P., Caramaschi, U., & Pinto, R. R. (2006). Redescription of *Leptotyphlops koppesi* Amaral, 1954, and description of a new species of the *Leptotyphlops dulcis* group from central Brazil (Serpentes: Leptotyphlopidae). *Amphetamine Reptile*, *27*, 347–357.

Persky, B., Smith, H. M., & Williams, K. L. (1976). Additional observations on ophidian costal cartilages. *Herpetologica*, *32*, 399–401.

Peters, W. C. (1858). Über die Typhlopinen oder blödsichtigen Schlangen und über neue dahin gehörige Arten. *Monatsberichte der königlichen Akademie der Wissenschaften zu Berlin*, *1857*, 508–509.

Pinto, R. R. (2010). *Revisão sistemática da Subtribo Renina (Serpentes: Leptodtyphlopidae)*. (Unpublished thesis). Museu Nacional /Universide Federal do Rio de Janeiro, Rio de Janeiro, Brazil.

Pinto, R., Passos, P., Portilla, J., Arredondo, J., & Fernandes, R. (2010). Taxonomy of the threadsnakes of the tribe Epictini (Squamata: Serpentes: Leptotyphlopidae) in Colombia. *Zootaxa*, *2724*, 1–28.

Pinto, R. R., & Curcio, F. (2011). On the generic identity of *Siagonodon brasiliensis*, with the description of a new leptotyphlopid from central Brazil (Serpentes: Leptotyphlopidae). *Copeia*, *2011*, 53–63.

Pinto, R. R., & Fernandes, R. (2012). A new blind snake species of the genus *Tricheilostoma* from Espinhaço range, Brazil and taxonomic status of *Rena dimidiata* (Jan, 1861) (Serpentes: Epictinae: Leptotyphlopidae). *Copeia*, *2012*, 37–48.

Pinto, R. P., Martins, A. R., Curcio, F. F., & Ramos, L. O. (2015). Osteology and cartilaginous elements of *Trilepida salgueiroi* Amaral, 1954 (Scolecophidia: Leptotyphlopidae). *The Anatomical Record*, *298*, 1722–1747.

Pinto, R., & Fernandes, R. (2017). Morphological variation of *Trilepida macrolepis* (Peters 1857), with reappraisal of the taxonomic status of *Rena affinis* (Boulenger 1884) (Serpentes: Leptotyphlopidae: Epictinae). *Zootaxa*, *4244*, 246–260.

Renous, S., & Gasc, J. (1991). Comments on the Pelvic Appendicular Vestiges in an Amphisbaenian: Blanus cinereus (Reptilia, Squamata), *209*, 23–38.

Rieppel, O. (1979). The braincase of *Typhlops* and *Leptotyphlops* (Reptilia: Serpentes). *Zoological Journal of the Linnean Society London*, *65*, 161–176.

Rieppel, O. (1988). A review of the origin of snakes. In M. Hecht, B. Wallace, & G. T. Prance (Eds.), *Evolutionary biology* (pp. 37–130). Boston, MA: Springer.

Rieppel, O., Kley, N. J., & Maisano, J. A. (2009). Morphology of the skull of the white-nosed blindsnake, *Liotyphlops albirostris* (Scolecophidia: Anomalepididae). *Journal of Morphology*, *270*, 536–557.

Romer, A. (1956). *Osteology of reptiles*. Chicago, CA: Krieger Pub Co.

Roscito, J. G., & Rodrigues, M. T. (2013). A comparative analysis of the post-cranial skeleton of fossorial and non-fossorial gymnophthalmid lizards. *Journal of Morphology*, *274*(8), 845–858. http://doi.org/10.1002/jmor.20139

Salazar-Valenzuela, D., Martins, A. R., Amador-Oyola, L., & Torres-Carvajal, O. (2015). A new species and country record of threadsnakes (Serpentes: Leptotyphlopidae: Epictinae) from northern Ecuador. *Amphibian & Reptile Conservation*, *8*, 107–120.

Song, J., & Parenti, L. (1995). Clearing and staining whole fish specimens for simultaneous demonstration of bone, cartilage, and nerve. *Copeia*, *1995*, 114–118.

Taylor, W. R., & Van Dyke, G. C. (1985). Revised procedures for staining and clearing small fishes and other vertebrates for bone and cartilage study. *Cybium*, *9*, 107–119.

Uetz, P., Freed, P., & Hosek, J. (2020). The reptile database. Retrieved from http://www.reptile-database.org

Underwood, G. (1967). *A contribution to the classification of snakes*. London: Trustees of the British Museum (Natural History).

Underwood, G. (1970). The eye. In C. Gans & T. S. Parsons (Eds.), *Biology of the Reptilia, Vol 2* (pp. 1–97). London, UK: Academic Press.

Van Devender, T. R., & Worthington, R. D. (1977). The herpetofauna of Howell's Ridge Cave and the paleoecology of the northwestern Chihuahuan Desert. In R. H. Wauer & D. H. Riskind (Eds.), *Transactions of the Symposium on the Biological Resources of the Chihuahuan Desert Region, US Mexico*. Washington, DC: National Park Service.

Van Devender, T. R., & Mead, J. I. (1978). Early Holocene and late Pleistocene amphibians and reptiles in Sonoran Desert packrat middens. *Copeia*, *1978*, 464–475.

Vidal, N., & Hedges, S. B. (2002). Higher-level relationships of snakes inferred from four nuclear and mitochondrial genes. *Comptes Rendus Biologies*, *325*, 977–985.

Wallach, V. (1998a). *The visceral anatomy of blindsnakes and wormsnakes and its systematic implications (Serpentes: Anomalepididae, Typhlopidae, Leptotyphlopidae)*. (Unpublished thesis). Boston.

Wallach, V. (1998b). The lungs of snakes. In C. Gans & A. S. Gaunt (Eds.), *Biology of the Reptilia* (Vol. 19, pp. 93–295). New York: Society for the Study of Amphibians and Reptiles.

Wallach, V. (2016). Morphological review and taxonomic status of the *Epictia phenops* species group of Mesoamerica, with description of six new species and discussion of South American *Epictia albifrons*, *E. goudotii*, and *E. tenella* (Serpentes: Leptotyphlopidae: Epictinae). *Mesoamerican Herpetology*, *3*, 215–374.

Wallach, V., Williams, K. L., & Boundy, J. (2014). *Snakes of the world: A catalogue of living and extinct species*. Florida: CRC Press.

Wake, M. H. (1993). The skull as a locomotor organ. In J. Hanken & B. K. Hall (Eds.), *The skull: Functional and evolutionary mechanisms, Vol 3* (pp. 197–240). Chicago, IL: University of Chicago Press.

How to cite this article: Martins, A., Koch, C., Joshi, M., Pinto, R., & Passos, P. (2021). Picking up the threads: Comparative osteology and associated cartilaginous elements for members of the genus *Trilepida* Hedges, 2011 (Serpentes, Leptotyphlopidae) with new insights on the Epictinae systematics. *The Anatomical Record*, 1–34. https://doi.org/10.1002/ar.24747

APPENDIX A.

MATERIAL EXAMINED

[1] μCT
[2] X-Ray
[3] Cleared and stained

Trilepida affinis ($n = 1$). VENEZUELA: TÁCHIRA: BMNH 1946.1.11.16[1,2] (holotype).

Trilepida brasiliensis ($n = 10$). BRAZIL: BAHIA: *Barreiras*: RBINS 2049.12594[1] (holotype). *Correntina*: MNRJ 18392[2]-93[2]. *Jaborandi*: 19484[2]-86[2]. MNRJ MATO GROSSO DO SUL: *Corumbá*: UFMT 1159[3], 1163[3]. *Rosário d'Oeste*: MNRJ 243341[1]. TOCANTINS: *Rio Sono*: MNRJ 24392[2].

Trilepida dimidiata ($n = 4$). BRAZIL: RORAIMA: *Boa Vista*: MZUSP 10090[3], 10120[1]. *Ilha de Maracá*: BMNH 1994.241[1]. GUIANA: LETHEM: *Karanamboo Ranch*: USNM 566291[2]

Trilepida fuliginosa ($n = 4$). BRAZIL: GOIÁS: *Luziânia*: CHUNB 40847[3]. *São domingos*: MNRJ 24401[2]. *Ouvidor*: MNRJ 19221[1], 19223[1].

Trilepida guayaquilensis ($n = 1$). ECUADOR: GUAYAS: Guayaquil: ZMB 4508[1,2] (holotype).

Trilepida jani ($n = 4$). BRAZIL: MINAS GERAIS: *Grão Mogol*: MNRJ 25148[2]. *Ouro Preto*: LZV 813S[3]. *Ouro Branco*: LZV778S[1]. *No locality*: MNRJ 16990[3]

Trilepida joshuai ($n = 3$). COLOMBIA: ANTIOQUIA: *Jericó*: IBSP 8919[1,3]. *Tocata*: NHMW 38424.1[2], 38424.2[1]

Trilepida koppesi ($n = 4$). BRAZIL: GOIÁS: *Aporé*: MNRJ 14116[2], 24715[3], 24716[1,] 24397[2], 24398[2]. *Luiziânia*: CHUNB40788[3]. *Mineiros*: CHUNB 25714[3]

Trilepida macrolepis ($n = 9$). BRAZIL: PARÁ: Parauapebas: *Floresta Nacional de Carajás*: MPEG 23017[1,3], *Vitória do Xingu*: MNRJ 25561[2]. COLOMBIA: VALLE

DEL CAUCA: *Buenaventura*: USNM 154031[2], 267261[2]. VENEZUELA: MIRANDA: *Caracas*: USNM 62205[2], 107891[2]. CARABOBO: Puerto Cabello: ZMB 1434[1,2] (lectotype), ZMB 5722[1,2], 5294[1,2] (paralectotypes).

Trilepida nicefori ($n = 1$). VENEZUELA: TÁCHIRA: *Bedriaga*: MNHN 1900.151[1,2]

Trilepida pastusa ($n = 1$). ECUADOR: CARCHI: *Tulcán*: QCAZ 5778[1] (paratype).

Trilepida salgueiroi ($n = 5$). BRAZIL: MINAS GERAIS: Aimorés: MCN-R 1468[3]. Muriaé: MZUFV 1519[3]. RIO DE JANEIRO: *Cambuci*: MNRJ 12132[3], 14487[1]. Niterói: 15422[3], 13124[3].